Latent Energy-Based Odyssey: Black-Box Optimization via Expanded Exploration in the Energy-Based Latent Space

Peiyu Yu 1* Dinghuai Zhang 2* Hengzhi He 1* Xiaojian Ma 4 Ruiyao Miao 1

Yifan Lu¹ Yasi Zhang¹ Deqian Kong¹ Ruiqi Gao³ Jianwen Xie⁵

Guang Cheng¹ Ying Nian Wu¹

¹University of California, Los Angeles ²Mila - Quebec AI Institute ³Google DeepMind ⁴Beijing Institute for General Artificial Intelligence (BIGAI) ⁵Akool Research

Abstract

Offline Black-Box Optimization (BBO) aims at optimizing a black-box function using the knowledge from a pre-collected offline dataset of function values and corresponding input designs. Prior works have made decent progress on i) forward approaches that learn surrogates to approximate the black-box function and optimize the surrogates w.r.t. input designs, and ii) inverse approaches that directly map the given function values to input designs. However, the high-dimensional and highly-multimodal input design space of black-box function pose inherent challenges for most existing methods that model and operate directly upon input designs. These issues include but are not limited to high sample complexity, which relates to inaccurate approximation of black-box function; and insufficient coverage and exploration of input design modes, which leads to suboptimal proposal of new input designs. In this work, we consider finding a latent space that serves as a compressed vet accurate representation of the design-value joint space, enabling effective latent exploration of high-value input design modes. To this end, we formulate an learnable energy-based latent space, and propose Noise-intensified Telescoping density-Ratio Estimation (NTRE) scheme for variational learning of an accurate latent space model without costly Markov Chain Monte Carlo. The optimization process is then exploration of high-value designs guided by the learned energy-based model in the latent space, formulated as gradient-based sampling from a latent-variable-parameterized inverse model. We show that our particular parameterization encourages expanded exploration around high-value design modes, motivated by inversion thinking of a fundamental result of conditional covariance matrix typically used for variance reduction. We observe that our method, backed by an accurately learned informative latent space and an expanding-exploration model design, yields significant improvements over strong previous methods on both synthetic and real world datasets such as the design-bench suite.

1 Introduction

Black-Box Optimization (BBO) problems are ubiquitous and fundamental in a wide range of science and engineer problems: protein [1, 2], molecule design [3–5] or designing controllers [6], etc.

^{*}Equal Contribution.

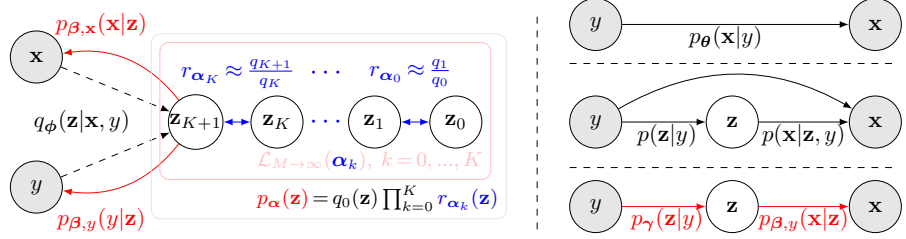


Figure 1: Graphical illustration of our framework LEO. We illustrate the learning scheme in the left panel. We construct an energy-based latent space model p_{α} for offline BBO via learning a series of ratio estimators $\{r_{\alpha_k}\}_{k=0}^K$ with the NTRE objective $\mathcal{L}_{M\to\infty}$ to optimize the ELBO without MCMC. We illustrate the optimization scheme in the right panel. After training, we solve offline BBO by sampling from the z-parameterized inverse model $p_{\theta}(\mathbf{x}|y) \propto \mathbb{E}_{p_{\gamma}(\mathbf{z}|y)}[p_{\beta,\mathbf{x}}(\mathbf{x}|\mathbf{z})]$, where $p_{\gamma}(\mathbf{z}|y) \propto p_{\beta,y}(y|\mathbf{z})p_{\alpha}(\mathbf{z})$ given y as the offline dataset maximum. Specifically, we first sample $\mathbf{z} \sim p_{\gamma}(\mathbf{z}|y)$, and then generate $\mathbf{x} \sim p_{\beta,\mathbf{x}}(\mathbf{x}|\mathbf{z})$. We provide previous parameterizations for the inverse model in the right panel for reference. Best viewed in color.

However, optimizing a black-box function in an excessively large search space is typically expensive [7, 8]; it often requires real-world experimentation and exploration of a very high-dimensional search space. Fortunately, for many such BBO problems, we often have access to an offline dataset of function values and corresponding input designs, which can greatly reduce the budget for costly online function evaluation if properly utilized. This introduces us to the offline BBO set-up (see Sec. 2), also known as Model-Based Optimization (MBO) in the literature [9–20].

Two broad classes of approaches have been proposed to address this fundamental research question. One line of research with abundant inspiring works [1,9-12] focuses on learning an inverse model $p_{\theta}(\mathbf{x}|y)$, i.e., a stochastic mapping from the function value y to the input design \mathbf{x} for offline BBO. The mapping is generally one-to-many as different input designs can have the same function value; an ideal inverse model should faithfully capture multiple possible modes of high-value input designs. For inverse models $p_{\theta}(\mathbf{x}|y)$, solving the BBO problem becomes sampling \mathbf{x} conditioned on a specific value of y to propose candidate input designs. On another front, forward approaches learn surrogate models to approximate the black-box function and have greatly pushed the boundries of offline BBO [13-18, 21, 22]. A properly learned forward model serves to optimize its input with gradient-based optimizers, or as a proxy oracle for a standard online BBO surrogate such as Bayesian Optimization (BO) [23-26] with a Gaussian Process. An interesting branch that shares the spirit of forward approaches is recently proposed in [19, 20]. Instead of learning the surrogate for gradient-based optimization, the methods seek to mimic the optimization trajectories with transformer-based models. We kindly refer to Appx. A for a more in-depth discussion of the related work.

Despite the exciting progress made by previous seminal works, the high-dimensional and highlymultimodal input design spaces of black-box functions inherently pose challenges for most existing methods that model and operate directly upon input designs. Some key challenges include but are not limited to: i) high sample complexity rooted in the high-dimensionality and multimodality of input design spaces, which can result in inaccurate approximations of black-box functions or optimization trajectories especially on out-of-distribution input designs [7, 10, 16–18, 22–25]; and ii) insufficient coverage and exploration of input design modes of the learned models, which leads to suboptimal proposal of new input designs [10, 11]. We provide two sets of proof-of-concept experiments in Appx. E.2.4 and Sec. 4.1 to show that these issues exist even for previous state-of-the-art methods employing modern transformer-based [19] or diffusion-based [11] models. On the other hand, the idea of introducing and operating in a compressed latent space has witnessed great successes in generative modeling of various complex data distributions including images, videos and text [27–38]. Specifically in the context of (online) BO, high-dimensional optimization is often reduced into lowdimensional independent or partially dependent sub-problems [39–41] to address the exponentially high sample complexity [7]; several pioneering works [23, 25, 42-45] also consider random or learned linear/non-linear mappings (e.g., Variational Auto-Encoder (VAE) [46, 47]) to exploit the intrinsic structure of the optimization problem for effective online exploration. Taking together, we are therefore motivated to find a latent space that serves as a compressed yet accurate representation of the input-design-function-value joint space, enabling effective latent exploration of high-value input design modes to solve the offline BBO problem.

Our proposed model shares the flavor of inverse approaches, while the model is parameterized by the latent variable z. Let $\theta = \{\alpha, \beta\}$, and α, β denote the parameters of latent space model and top-down

model (decoder that maps the latent variables back to input design space). Particularly, we consider $p_{\theta}(\mathbf{x}|y) \propto \int_{\mathbf{z}} p_{\beta}(\mathbf{x},y|\mathbf{z}) p_{\alpha}(\mathbf{z}) d\mathbf{z} = \int_{\mathbf{z}} p_{\beta,\mathbf{x}}(\mathbf{x}|\mathbf{z}) p_{\beta,y}(y|\mathbf{z}) p_{\alpha}(\mathbf{z}) d\mathbf{z} \propto \mathbb{E}_{p_{\gamma}(\mathbf{z}|y)}[p_{\beta,\mathbf{x}}(\mathbf{x}|\mathbf{z})]$ with the Bayes rule, where $p_{\gamma}(\mathbf{z}|y) \propto p_{\beta,y}(y|\mathbf{z}) p_{\alpha}(\mathbf{z})$. Our core assumption here is the conditional independence of \mathbf{x} and y given \mathbf{z} , *i.e.*, \mathbf{z} sufficiently encodes the joint information of (\mathbf{x},y) so that $p_{\beta}(\mathbf{x},y|\mathbf{z}) = p_{\beta,\mathbf{x}}(\mathbf{x}|\mathbf{z}) p_{\beta,y}(y|\mathbf{z})$. Intuitively, our inverse model for offline BBO, $\mathbb{E}_{p_{\gamma}(\mathbf{z}|y)}[p_{\beta,\mathbf{x}}(\mathbf{x}|\mathbf{z})]$, can be viewed as a delicate symbiosis between exploitation of the offline high value design modes, $p_{\gamma}(\mathbf{z}|y)$, and guided exploration around these modes in the latent space, $p_{\beta,\mathbf{x}}(\mathbf{x}|\mathbf{z})$, $\mathbf{z} \sim p_{\gamma}(\mathbf{z}|y)$. We show that (see Secs. 3.3 and 4) this particular choice of parameterization, motivated by inversion thinking of a fundamental result of conditional covariance matrix, brings extra exploratory ability and leads to better proposed designs over previous model designs of inverse approaches; these alternative design choices (see Fig. 1) include directly modeling $p_{\theta}(\mathbf{x}|y)$ in the input design space (e.g., [11]) and modeling without the conditional independence assumption, *i.e.*, $p_{\theta}(\mathbf{x}|y) \propto \mathbb{E}_{p(\mathbf{z}|y)}[p(\mathbf{x}|\mathbf{z},y)]$ (e.g., [10]). To ensure accurate modeling of offline high value design modes using $p_{\theta}(\mathbf{z}|y) \propto p_{\beta,y}(y|\mathbf{z})p_{\alpha}(\mathbf{z})$, we formulate an energy-based latent space model $p_{\alpha}(\mathbf{z})$ due to its superior flexibility and expressive power [27, 29, 30].

A naive way for variational learning [46] of the latent space optimizes the following ELBO,

$$ELBO_{\boldsymbol{\theta}, \boldsymbol{\phi}} = \mathbb{E}_{q_{\boldsymbol{\phi}}(\mathbf{z}|\mathbf{x}, y)}[\log p_{\boldsymbol{\beta}}(\mathbf{x}, y|\mathbf{z})] - \mathbb{D}_{KL}(q_{\boldsymbol{\phi}}(\mathbf{z}|\mathbf{x}, y)||p_{\boldsymbol{\alpha}}(\mathbf{z})), \tag{1}$$

where in $p_{\theta}(\mathbf{x}, y)$, $p_{\beta, \mathbf{x}}(\mathbf{x}|\mathbf{z}) = \mathcal{N}(g_{\beta, \mathbf{x}}(\mathbf{z}), \sigma_x^2 \mathbf{I})$ for continuous \mathbf{x} and multinomial for discrete \mathbf{x} , and $p_{\beta, y}(y|\mathbf{z}) = \mathcal{N}(g_{\beta, y}(\mathbf{z}), \sigma_y^2 \mathbf{I})$. $g_{\beta, \mathbf{x}}$ and $g_{\beta, y}$ is the generator network for \mathbf{x} and prediction network for y, respectively. σ_x^2, σ_y^2 take pre-specified values. $q_{\phi}(\mathbf{z}|\mathbf{x}, y) = \mathcal{N}(\mu_{\phi}, \sigma_{\phi} \mathbf{I})$ is the amortized posterior. This naive solution, however, does not work well in the offline BBO setting (see Tab. 4), as learning this latent space model typically requires Markov Chain Monte Carlo (MCMC) sampling [27]. As pointed out in [30, 48], the sampling quality of MCMC can drastically degenerate in practice [49–53], especially on data with complex latent structures; this phenomenon is particularly concerning in variational learning of model parameters. Inspired by [54], in this work we consider forming an energy-based latent space with a novel Noise-intensified Telescoping density-Ratio Estimation (NTRE) scheme for offline BBO; the non-trivial connection between the gradient of maximizing Eq. (1) and that of the proposed NTRE objective completely frees us from the commonly-used yet often costly and biased MCMC. Finally, with the properly learned models, we formulate the optimization process as gradient-based sampling, instantiated as Stein Variational Gradient Descent (SVGD) pull-backed to the latent space. We term the resulting framework as Latent Energy-based Odyssey (LEO) (see Fig. 1) highlighting each component in our model design.

Contributions (i) We introduce a novel framework, LEO, backed by an accurately learned informative latent space and an expanding-exploration model design for solving the offline BBO problem. We offer theoretical evidence that the proposed parameterization of inverse model brings extra exploratory ability. (ii) We propose a MCMC-free scheme for learning an energy-based latent space, potentially applicable to a wider range of generative modeling tasks. We provide theoretical discussion of the corresponding objective. (iii) Experimentally, we observe LEO yields significant improvements over strong baselines on the design-bench suite [21], confirming the effectiveness of our framework.

2 Preliminaries

Problem statement Let $h: \mathcal{X} \to \mathbb{R}$ be a scalar function; the domain \mathcal{X} is an arbitrary subset of \mathbb{R}^d . In BBO, h is an unknown black-box function; we are interested in finding \mathbf{x}^* that maximizes h:

$$\mathbf{x}^* \in \operatorname*{arg\,max}_{\mathbf{x} \in \mathcal{X}} h(\mathbf{x}). \tag{2}$$

Typically, h is expensive to evaluate. In offline BBO, we assume no direct access to h during training, and are thus **not allowed** to actively query the black-box function during optimization, unlike in online BBO where most approaches would employ iterative online solving schemes [5, 4, 7, 55]. Specifically, in the *offline* BBO setting [21], one has only access to a pre-collected dataset of observations, $\mathcal{D} = \{(\mathbf{x}_i, y_i)\}_{i=1}^n$, where $h(\mathbf{x}_i) = y_i$. During evaluation, one may query the function h for a small budget of Q queries to output candidates with the best function value obtained.

Latent-space Energy-Based Model (LEBM) We refer to the energy-based parameterization of the latent space model $p_{\alpha}(\mathbf{z})$ [27] as LEBM throughout the paper:

$$p_{\alpha}(\mathbf{z}) := \frac{1}{Z_{\alpha}} \exp(f_{\alpha}(\mathbf{z})) q_0(\mathbf{z}). \tag{3}$$

 $f_{m{lpha}}({f z})$ is parameterized by a neural network with scalar output, $Z_{m{lpha}}$ is the partition function, and $q_0({f z})$ is standard Gaussian as the base distribution. The model in Eq. (3) can be interpreted as an energy-based correction or exponential tilting of q_0 [49]. Typically, ${m{lpha}}$ can be estimated through Maximum Likelihood Estimation (MLE) with posterior samples, requiring MCMC such as Langevin Dynamics (LD) [27, 56]: ${f z}^{t+1} = {f z}^t + \frac{\epsilon^2}{2} \nabla_{{f z}^t} l({f z}^t) + \epsilon {f w}^t, \ t=0,1,...,T-1, \ {f w}^t \sim \mathcal{N}({f 0},{f I})$, where ϵ is the step size, and $l({f z})$ is the log-density function.

Noise Contrastive Estimation (NCE) An alternative approach to MLE is converting the estimation of α into a classification problem. Suppose we have q^* as the target distribution and q_0 as the base distribution. Instead of directly modeling p_{α} to approximate q^* , we can estimate the density-ratio $r_{\alpha} = p_{\alpha}/q_0$ by distinguishing samples from q^* and q_0 [57–59]. For a correctly specified model, the optimal ratio satisfies $r_{\alpha^*} \approx q^*/q_0, p_{\alpha^*} \approx q^*$. There are many choices for the loss function of the classification problem [60–63]; abundant seminal works focus on the logistic loss as follows

$$\mathcal{L}(\alpha) = \mathbb{E}_{q^*(\mathbf{z})} \left[\log \frac{r_{\alpha}(\mathbf{z})}{1 + r_{\alpha}(\mathbf{z})} \right] + \mathbb{E}_{q_0(\mathbf{z})} \left[\log \frac{1}{1 + r_{\alpha}(\mathbf{z})} \right]. \tag{4}$$

The original formulation in Telescoping Density Ratio Estimation (TRE) [54] also focuses on Eq. (4), while we study a noise-intensified variant (Gutmann and Hyvärinen [59], see Eq. (9)). We will see the importance of base distribution intensity in NTRE later in Sec. 3.1.

Stein Variational Gradient Descent (SVGD) A well-established technique for sampling from the target distribution is SVGD, first proposed in the seminal work of [64]. Given an unnormalized log-density function $l(\mathbf{z})$, and an initial set of samples $\{\mathbf{z}_i^0\}_{i=1}^n$, one can update the set as follows to approximately draw samples from the distribution:

$$\mathbf{z}_{i}^{t+1} = \mathbf{z}_{i}^{t} + \epsilon_{t} \hat{\phi}^{*}(\mathbf{z}_{i}^{t}), \ t = 0, 1, ..., T - 1; \text{ where } \hat{\phi}^{*}(\mathbf{z}) = \frac{1}{n} \sum_{j=1}^{n} \left[k(\mathbf{z}_{j}^{t}, \mathbf{z}) \nabla_{\mathbf{z}_{j}^{t}} l(\mathbf{z}_{j}^{t}) + \nabla_{\mathbf{z}_{j}^{t}} k(\mathbf{z}_{j}^{t}, \mathbf{z}) \right],$$

$$(5)$$

where $k(\cdot, \cdot)$ is a positive definite kernel (e.g., RBF kernel) and ϵ_t the step size at the t-th iteration. We formulate the optimization process as sampling from $p_{\gamma}(\mathbf{z}|y)$ and utilize the exploration ability of our model design to propose high-quality candidates for the BBO problem.

3 Latent Energy-based Odyssey (LEO)

3.1 Energy-Based Latent Space Induced by NTRE

Inspired by Rhodes et al. [54], we propose to parameterize the prior model as

$$p_{\alpha}(\mathbf{z}) = q_0(\mathbf{z}) \prod_{k=0}^{K} r_{\alpha_k}(\mathbf{z}), \tag{6}$$

where we learn an ensemble of ratio estimators $\{r_{\alpha_k}\}_{k=0}^K$ to construct a LEBM $p_{\alpha}(\mathbf{z})$ approximating the target distribution in the latent space, denoted as q_{K+1} . We consider decomposing this ratio estimation problem between q_{K+1} and q_0 into a telescoping product $\frac{q_{K+1}}{q_0} = \frac{q_{K+1}}{q_K} \frac{q_K}{q_{K-1}} \cdots \frac{q_1}{q_0}$, where $\{q_k\}_{k=1}^K$ are pre-specified intermediate target distributions. This particular decomposition consequently leads to a fruitful collection of intermediate ratios, where each pair of distributions q_{k+1} and $q_k, k=0,...,K$ has larger overlap compared with the initial ratio q_{K+1}/q_0 , resulting in easier-to-learn ratio estimators [54]. To construct these intermediate distributions, we follow [30] to spherically interpolates between pairs of samples $\mathbf{z}_{K+1} \sim q_{K+1}$ and $\mathbf{z}_0 \sim q_0$; samples from the k-th intermediate distribution q_k are: $\mathbf{z}_k = \sqrt{1-\sigma_k^2}\mathbf{z}_0 + \sigma_k\mathbf{z}_{K+1}$, where the $\{\sigma_k\}_{k=1}^K$ form an increasing sequence from 0 to 1. Particularly, building upon $\{q_k\}_{k=1}^K$, we design the ratio estimator for each stage as $r_{\alpha_k} = \frac{p_{\alpha_k}}{q_k}$, i.e., ratio between an implicitly learned energy-based distribution p_{α_k} and q_k . Ideally, with a correctly specified training objective, the optimum of this model is $r_{\alpha_k}^* = q_{k+1}/q_k$ or equivalently $p_{\alpha_k}^* = q_{k+1}, k = 0, ..., K$. Therefore, we can closely approximate the target distribution as $q_{K+1} \approx \left(\frac{p_{\alpha_K}}{q_K}\right)\left(\frac{p_{\alpha_{K-1}}}{q_{K-1}}\right)\cdots\left(\frac{p_{\alpha_0}}{q_0}\right)q_0 = q_0\prod_{k=0}^K r_{\alpha_k}$ with a properly designed objective.

Although our parameterization of $p_{\alpha}(\mathbf{z})$ shares the same spirit as in Rhodes et al. [54], the learning method and objective are fundamentally different, which we will show below. We can first see that

the target distribution for p_{α} is the aggregated posterior [65] $q_{K+1}(\mathbf{z}) = \int_{\mathbf{x},y} q_{\phi}(\mathbf{z}|\mathbf{x},y)p(\mathbf{x},y)d\mathbf{x}dy$ from Eq. (1). Since we now consider an ensemble of the ratio estimators, we can plug Eq. (6) and additional Kullbeck-Leibler Divergence (KLD) terms into the vanilla ELBO in Eq. (1) to further optimize the following lower bound involving ratio estimators:

$$ELBO_{re,\boldsymbol{\theta},\boldsymbol{\phi}} = \mathbb{E}_{q_{\boldsymbol{\phi}}}[\log p_{\boldsymbol{\beta}}(\mathbf{x}, y | \mathbf{z})] - \mathbb{D}_{KL}(q_{\boldsymbol{\phi}} || r_{\boldsymbol{\alpha}_K} q_K) - \sum_{k=0}^{K-1} \mathbb{D}_{KL}(q_{k+1} || r_{\boldsymbol{\alpha}_k} q_k), \tag{7}$$

which is a valid ELBO by the definition of our latent space model in Eq. (6) and non-negativity of the KLD. Inserting the energy-based parameterization of $p_{\alpha_k}(\mathbf{z})$ into each ratio estimator, *i.e.*, $p_{\alpha_k}(\mathbf{z}) = Z(\alpha_k)^{-1} \exp\left(f_{\alpha_k}(\mathbf{z})\right) q_k(\mathbf{z})$, we can derive the gradient that optimizes Eq. (7) for each r_{α_k} as (see Appx. B.1 for detailed derivation and discussions)

$$\nabla_{\alpha_k} \operatorname{ELBO}_{re} = \mathbb{E}_{q_{k+1}} [\nabla_{\alpha_k} f_{\alpha_k}(\mathbf{z})] - \mathbb{E}_{p_{\alpha_k}} [\nabla_{\alpha_k} f_{\alpha_k}(\mathbf{z})]. \tag{8}$$

Typically, calculating the gradient in Eq. (8) requires MCMC sampling for approximation of the expectation. Fortunately, however, it can be shown that optimizing the following Noise-intensified Telescoping density-Ratio Estimation (NTRE) objective equivalently provides the gradient for estimating $\{r_{\alpha_k}\}_{k=0}^K$, when M is large enough:

$$\mathcal{L}_{M}(\boldsymbol{\alpha}_{k}) = \mathbb{E}_{q_{k+1}} \left[\log \frac{r_{\boldsymbol{\alpha}_{k}}}{M + r_{\boldsymbol{\alpha}_{k}}} \right] + M \mathbb{E}_{q_{k}} \left[\log \frac{M}{M + r_{\boldsymbol{\alpha}_{k}}} \right]. \tag{9}$$

The objective in Eq. (9) can be seen as a variant of Eq. (4), while the intensity of base distribution is further modulated by the factor M. Particularly, as $M \to \infty$, the gradient of Eq. (9) converges to Eq. (8). This provides us with a very useful interface to calculate the gradient for $\{r_{\alpha_k}\}_{k=0}^K$ that optimizes the ELBO involving informative prior model *without* resorting to MCMC. Formally:

Proposition 3.1. (Approx. grad.) As
$$M \to \infty$$
, $\nabla_{\alpha_k} \mathcal{L}_M(\alpha_k) \to \nabla_{\alpha_k} \text{ELBO}_{\text{re}}$.

Remark 3.2. Proposition 3.1 is a modified version of the results in [66], where the initial idea was for fitting the word embedding of context-dependent models. It can be shown that $\nabla_{\alpha_k} \mathcal{L}_M(\alpha_k) = \int_{\mathbf{z}} \frac{M}{r_{\alpha_k}(\mathbf{z}) + M} \left(q_{k+1}(\mathbf{z}) - p_{\alpha_k}(\mathbf{z})\right) \nabla_{\alpha_k} f_{\alpha_k}(\mathbf{z}) d\mathbf{z}$. Thus the gradient in Eq. (8) can be approximated with sufficiently large M. Since each estimator r_{α_k} addresses a sub-problem $\frac{p_{\alpha_k}}{q_k} \approx \frac{q_{k+1}}{q_k}$, where the distributions have significant overlap, M does not need to be very large for $\frac{M}{r_{\alpha_k} + M} \approx 1$. In practice, we observe M = 100 produces decent results. We refer to Appx. B.2 and E.2.4 for the full derivation and further discussion of this approximation; Sec. 3.3 discusses theoretical properties of Eq. (9).

3.2 How to LEO: Algorithms and Implementation

Optimization as gradient-based sampling Once the latent space model p_{α} is properly trained with NTRE, we can sample from the parameterized inverse model $p_{\theta}(\mathbf{x}|y) \propto \mathbb{E}_{p_{\gamma}(\mathbf{z}|y)}[p_{\beta,\mathbf{x}}(\mathbf{x}|\mathbf{z})]$ to solve the BBO problem. Specifically, we i) sample \mathbf{z} from $p_{\gamma}(\mathbf{z}|y) \propto p_{\beta,y}(y|\mathbf{z})p_{\alpha}(\mathbf{z})$ with SVGD, where y is set to the offline dataset maximum y_{\max} as in [11]; and ii) feed them into the generator network $g_{\beta,\mathbf{x}}$ to obtain the proposed input designs \mathbf{x} . Intuitively, $p_{\gamma}(\mathbf{z}|y=y_{\max})$ exploits the offline high value input design modes, while sampling from p_{γ} and mapping from z to x with $p_{\beta,\mathbf{x}}(\mathbf{x}|\mathbf{z})$ achieves expanded latent exploration guided by the latent space model p_{α} . We provide an interpretation of latent exploration in Appx. \mathbf{C} , and discussions of expanded exploration with $p_{\beta,\mathbf{x}}(\mathbf{x}|\mathbf{z})$ in Sec. 3.3.

Training and optimization algorithms As mentioned in Sec. 3.1, we directly learn the log-ratio estimator $\tilde{f}_{\alpha_k} = \log r_{\alpha_k}$ for implementation. Let $\sigma(\cdot)$ denote the sigmoid function, the gradient for learning each ratio estimator p_{α_k} , k = 0, 1, ..., K can be derived from Eq. (9) as:

$$\nabla_{\boldsymbol{\alpha}_{k}} \; \mathrm{ELBO} \approx \nabla_{\boldsymbol{\alpha}_{k}} \; \left\{ \mathbb{E}_{q_{k+1}} \; \left[\log \sigma \left(\tilde{f} \boldsymbol{\alpha}_{k}(\mathbf{z}) - \log M \right) \right] + M \mathbb{E}_{q_{k}} \left[\log \left(1 - \sigma \left(\tilde{f}_{\boldsymbol{\alpha}_{k}}(\mathbf{z}) - \log M \right) \right) \right] \right\}. \tag{10}$$

Let $\psi = \{\beta, \phi\}$ collect the parameters of the inference and generator networks. For q_{ϕ} and p_{β} , we can calculate the learning gradient as follows:

$$\nabla_{\boldsymbol{\psi}} \operatorname{ELBO}_{re} = \nabla_{\boldsymbol{\psi}} \mathbb{E}_{q_{\boldsymbol{\phi}}} [\log p_{\boldsymbol{\beta}}(\mathbf{x}, y | \mathbf{z})] - \nabla_{\boldsymbol{\phi}} \mathbb{D}_{\mathrm{KL}} (q_{\boldsymbol{\phi}}(\mathbf{z} | \mathbf{x}, y) || p_{0}(\mathbf{z})) - \nabla_{\boldsymbol{\phi}} \mathbb{E}_{q_{\boldsymbol{\phi}}} \left[\sum_{k=0}^{K} \tilde{f}_{\boldsymbol{\alpha}_{k}}(\mathbf{z}) \right]. \tag{11}$$

Algorithm 1: Learning & Opt. Algo. for LEO

```
Input: \mathcal{D}: \{\mathbf{x}^{(i)}, y^{(i)}\}_{i=1}^N, init. params. (\{\boldsymbol{\alpha}_k\}_{k=0}^K, \boldsymbol{\beta}, \boldsymbol{\phi}), train iter. M; init. \{\mathbf{z}_i^0\}_{i=1}^Q, SVGD iter. T.
    Output: updated params. (\{\alpha_k^*\}_{k=0}^K, \beta^*, \phi^*), the proposed candidate design set \{\mathbf{x}^{*(i)}\}_{i=1}^Q
1 Phase 1: Offline Training
2 for m = 0: M - 1 do
           Posterior sampling: For each pair of \{\mathbf{x}^{(i)}, y^{(i)}\}, sample \mathbf{z}_{K+1}^{(i)} \sim q_{\phi}(\mathbf{z}|\mathbf{x}^{(i)}, y^{(i)}).
           Forming \{q_k\}_{k=1}^K: For each sample \mathbf{z}_{K+1}^{(i)}, sample k \sim \mathrm{Unif}(\{0,...,K\}) and obtain
            \left(\mathbf{z}_k^{(i)}, \mathbf{z}_{k+1}^{(i)}\right) \sim (q_k, q_{k+1}) \text{ using } \mathbf{z}_k = \sqrt{1 - \sigma_k^2} \mathbf{z}_0 + \sigma_k \mathbf{z}_{K+1}.
           Learning \{\alpha_k\}_{k=0}^K: Update \{\alpha_k\}_{k=0}^K with Eq. (10). Learning \psi = (\beta, \phi): Update \psi with Eq. (11).
```

- 7 Phase 2: Optimization as Sampling
- 8 Latent exploitation-exploration: Sample $z \sim p_{\gamma}(\mathbf{z}|y=y_{\text{max}})$ with SVGD (Eq. (5)), updating $\{\mathbf{z}_i^0\}_{i=1}^Q$ to obtain $\{\mathbf{z}_i^T\}_{i=1}^Q$ as samples from $p_{\gamma}(\mathbf{z}|y=y_{\max})$.

 9 Expanded exploration: Return $\{\mathbf{x}_i^{*(i)}\}_{i=1}^Q = g_{\boldsymbol{\beta},\mathbf{x}}(\{\mathbf{z}_i^T\}_{i=1}^Q)$ to sample $\mathbb{E}_{p_{\gamma}(\mathbf{z}|y)}[p_{\boldsymbol{\beta},\mathbf{x}}(\mathbf{x}|\mathbf{z})]$.

After training, we can set $l(\mathbf{z}) = -\lambda_1 \|y_{\max} - g_{\boldsymbol{\beta},y}(\mathbf{z})\|_2^2 + \lambda_2 \left(\sum_{k=0}^K \tilde{f}_{\boldsymbol{\alpha}_k}(\mathbf{z}) - \frac{1}{2}\|\mathbf{z}\|_2^2\right)$, and use Eq. (5) to update an initial set of latent variable samples $\{\mathbf{z}_i^0\}_{i=1}^{N=Q}$ with the set size as the query budget Q allowed during evaluation. Alg. 1 summarizes the training and optimization algorithms.

Implementation Optimizing the ELBO_{re} in Eq. (7) requires joint optimization over all log-ratio estimators. To simplify and accelerate the training process, we randomly choose one intermediate stage to optimize at each training iteration as in [67]. In addition, we re-weight the objective for each α_k with $w_k = \sqrt{\sigma_K/\prod_{i=k}^K \sigma_i}$ to further emphasize stages closer to the final target distribution q_{K+1} , as in [30]. We use a shared network $\tilde{f}_{\alpha}(\mathbf{z},k)$ for each stage. The index k is encoded by sinusoidal position embedding; we use the linear schedule as in [67] to specify σ_k^2 and construct the intermediate distributions $\{q_k\}_{k=0}^K$. We set the number of stages K+1=6, and the number of SVGD iters T to 500 for all experiments. We use a 3-layer MLP and a 5-layer MLP for encoder and decoder networks. Continuous inputs are normalized to the [-1, 1] for each dimension. We add an additional embedding layer in encoders for discrete inputs. We kindly refer to Appx. D for further details.

3.3 Theoretical Understanding

We are now ready to provide some theoretical understanding about our framework. We first show that our particular parameterization of the inverse model $\mathbb{E}_{p_{\gamma}(\mathbf{z}|\mathbf{y})}[p_{\beta,\mathbf{x}}(\mathbf{x}|\mathbf{z})]$ encourages expanded exploration around high-value design modes. To this end, we propose a type of order relation to measure the exploratory ability of different distributions:

Definition 3.3. For two distributions p_A and p_B , we say that p_B is more exploratory than p_A if and only if $\forall 0 < \alpha < 1$, there exists two sets M, N and a vector μ , such that $p_A(M) = p_B(N) = \alpha$, and $\phi(M) + \mu \subset N$, where ϕ is a rotation transformation.

Theorem 3.4. $p_{\beta,\mathbf{x}}(\mathbf{x}|z)$ is more exploratory than $p_{\beta,\mathbf{x}}(\mathbf{x}|y,z)$ if $p_{\beta}(\mathbf{x},y|z)$ is jointly normal.

Remark 3.5. Theorem 3.4 states that the proposed parameterization $\mathbb{E}_{p_{\gamma}(\mathbf{z}|y)}[p_{\beta,\mathbf{x}}(\mathbf{x}|\mathbf{z})]$ is more exploratory than the one without conditional independence, $p_{\theta}(\mathbf{x}|y) \propto \mathbb{E}_{p(\mathbf{z}|y)}[p(\mathbf{x}|\mathbf{z},y)]$ (e.g., [10]). The discussion of Theorem 3.4 (see proof in Appx. B.3) provides theoretical evidence for continuous x; empirical results in Sec. 4.2 also confirms the advantages of our model design on discrete datasets. Directly modeling $p_{\theta}(\mathbf{x}|y)$ (e.g., [11]) without introducing z does not guarantee the exploratory ability, as the optimally learned model should faithfully reproduce the offline dataset.

We next show that the proposed NTRE objective helps to learn an accurate $p_{\alpha}(\mathbf{z})$ latent space model, facilitating exploitation and exploration of high value input design modes.

Proposition 3.6. (Optimal ratio) The optimal ratio estimator for each stage remains $r_{\alpha_k}^*(\mathbf{z}) = \frac{q_{k+1}(\mathbf{z})}{q_k(\mathbf{z})}$ and that $p_{\alpha_k}^*(\mathbf{z}) = q_{k+1}(\mathbf{z})$, regardless of the value of M.

Remark 3.7. Proposition 3.6 states that one can safely increase the intensity of the base distribution, M, while still recovering the correct target distribution with Eq. (9). See detailed proof in Appx. B.4. **Theorem 3.8.** (Informal) Under some regularity assumptions and given the initial and target parameters α_k^0 and α_k^* , performing normalized gradient descent on the Eq. (9) objective guarantees that when taking $T \leq \left(\frac{\lambda_{\max}}{\lambda_{\min}}\right)^3 \frac{\|\boldsymbol{\alpha}_k^0 - \boldsymbol{\alpha}_k^*\|_2^2}{\delta^2}$ steps, there exists $t \leq T$ such that $\|\boldsymbol{\alpha}_k^t - \boldsymbol{\alpha}_k^*\|_2 \leq \delta$.

Remark 3.9. Theorem 3.8 shows that the NTRE objective has a desirable convergence rate on exponential families parameterized by $\{\alpha\}_{k=0}^K$. The result stems but differs from the result in [68]. Typically, the convergence rate for the NCE-like objective is highly dependent on the condition number of the objective Hessian at the optimum. The growth of this condition number is unclear for arbitrary target and base distributions, unless they are sufficiently close. We show that, however, the condition number of the NTRE objective can be bounded under the same assumptions as in Liu et al. [68] without further requiring the closeness of distributions. This indicates that the base distribution itself actually serves as a good source for regularization, which is consistent with the results in [59, 69]. The full proof and the detailed formal statement can be found in Appx. B.5.

4 Experiments

4.1 2D Branin Function

We first evaluate our method with the 2D Branin function (Fig. 3) as a sanity check (see Appx. E.1 for more details) to validate our proposal. To show that our framework LEO can indeed generalize beyond the dataset maximum, we follow [11] to uniformly sample N=5000 points in the domain of $\mathbf{x} \in [-5,10] \times [0,15]$ to construct the offline dataset; we remove the top 10%-tile (according to the function value) from this set to make sure the global optima are unseen during training. During evaluation, we assume a query budget of 128. As shown in Tab. 1, LEO successfully generalizes beyond the best point in our offline dataset \mathcal{D}_{\max} , approaching the global optimal OPT . We include a Gradient Ascent (GA) baseline as well as BONET [19] and DDOM [11] for comparison. We can see that BONET and DDOM baselines perform reasonably well in this toy example, while still falling behind compared with our method. We will see in Sec. 4.2 that this advantage can be transferred and even exaggerated in larger-scale design-bench tasks.

Table 1: Results on the top-10%-tile-removed Branin task (averaged over 5 runs). We highlight our model, the $\mathbf{1}^{st}$ and $\underline{2^{nd}}$ performances; tables henceforth follows this format.

$\mathcal{D}_{\mathrm{max}}$ /Opt.	GA	BONET	DDOM	Ours
-6.119/-0.398	$-3.953_{\pm 4.258}$	$-1.790_{\pm0.843}$	$-1.585_{\pm 0.038}$	$-0.438_{\pm0.124}$
0 — mean — glabal min glabal max — glabal min — glabal min — glabal max — 100 — 110 — 120 — 120 — 120 — 130 — 1,0 — 0,5	** y cond. 65 1.0	-100 -100 -100 -100 -200 -200 -100	y cond.	maaa max dat max gadal max
(a) w/t	op-10% points	s (t	o) w/o top-109	% points

Figure 2: **Results of our method on uniformly sampled branin dataset** w/ and w/o top-10% points. Zoom-in for more details.

We next examine how well the latent space induced by Eq. (9) i) covers multiple modes of the offline high value designs (Fig. 4), and ii) models the implicit and intricate correlation between x and y (Fig. 2). We draw 2560 samples from each inverse model with $y_{\rm max}$ as the condition to visualize the results in Fig. 4. In Fig. 4(a), we emulate the distribution of true optimal points with a 3-component equi-weight GMM. We set the GMM means as the global optima in Fig. 3. We can see in the first row that as M gradually increases, the points proposed by our method approximates the groundtruth distribution increas-

ingly well. This confirms our analysis in Sec. 3.1 that M in Eq. (9) should be large enough to properly approximate the gradient in Eq. (8). Additionally, we can see that: i) state-of-the-art models like DDOM operating in the data space can sometimes miss critical modes of the distribution (Fig. 4(e)), and ii) the latent space cannot be fully captured with a non-informative Gaussian prior (Fig. 4(f)). These observations motivate the need of a learned informative latent space for BBO. In Fig. 4(g) and 4(h), we show empirically that vanilla MLE learning of the latent space fails to produce desirable results even on the 2D toy task. This is probably due to the intricate correlation between \mathbf{x} and y, which adds on extra burden to modeling the joint latent space. Fig. 2 shows the strong correlation between proposed function values and the conditioned y values in the proposed inverse model

 $\mathbb{E}_{p_{\gamma}(\mathbf{z}|y)}[p_{\beta,\mathbf{x}}(\mathbf{x}|\mathbf{z})]$; this confirms that the latent space induced by NTRE accurately encodes the joint information of \mathbf{x} and y. We can also see that this correlation successfully extrapolates beyond the offline dataset maximum in Fig. 2(b).

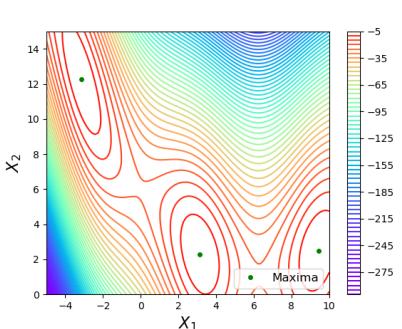


Figure 3: Branin function level sets.

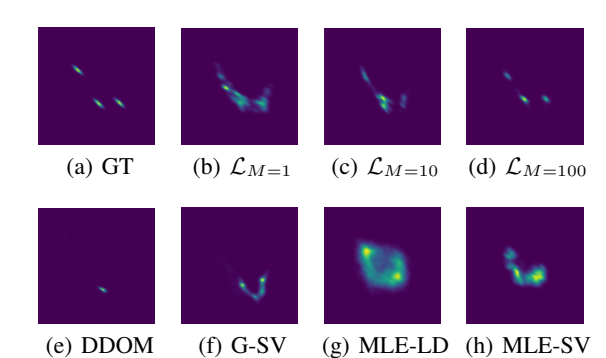


Figure 4: **Viz. of Branin samples.** (b-d) are results of our method. G-SV denotes the Gaussian prior model sampled with SVGD. MLE-LD and MLE-SV denote the LEBM trained by MLE sampled with LD and SVGD, respectively.

4.2 Offline BBO on Design-Bench

Task overview, Baselines and Evaluation Following [11], we test our method on high-dimensional real-world tasks² from [21] in two groups: discrete tasks including **TF-Bind-8**, **TF-Bind-10** and **ChEMBL**, and continuous tasks including **D'Kitty**, **Ant Morphology** and **Superconductor**. We compare our method with three groups of baselines: i) sampling via generative inverse models with different parameterizations, including CbAS [1], Auto.CbAS [9], MIN [10] and DDOM to validate our model design; ii) gradient(-like) updating from existing designs, *e.g.*, GA-based [13–18, 22] and BONET and iii) baselines mentioned in [21]. We refer to Appx. E.2.1 and E.2.3 for more details.

Following previous works [11, 18, 19, 21], we report the normalized ground truth function value as $y_n = \frac{y - y_{\min}^*}{y_{\max}^* - y_{\min}^*}$. y_{\min}^* and y_{\max}^* denote the lowest and the highest values in the full dataset unseen during training. We further report the mean scores and mean ranks (MNR) of the compared algorithms across tasks to measure the overall performance. We include two sets of major results: the first one follows the same evaluation protocol as in [11, 19] with a query budget Q = 256; the second one uses Q = 128 [14–18, 22], but excludes the **ChEMBL** dataset. We report the 100-th percentile results in the main text, and refer to Appx. E.2.4 for further results at 50-th and other percentiles.

Table 2: Normalized design-bench results with $Q=256$. Baseline numbers from [11].

BASELINE	TFBIND8	TFBIND10	CHEMBL	SUPERCON.	ANT	D'KITTY	MEAN SCORE [↑]	MNR^{\downarrow}
\mathcal{D} (best)	0.439	0.467	0.605	0.399	0.565	0.884	-	-
GP-qEI CMA-ES REINFORCE	0.824 ± 0.086 0.933 ± 0.035 0.959 ± 0.013	0.635 ± 0.011 0.679 ± 0.034 0.640 ± 0.028	0.633 ± 0.000 0.636 ± 0.004 0.636 ± 0.023	0.501 ± 0.021 0.491 ± 0.004 0.481 ± 0.017	0.887 ± 0.000 1.436 ± 0.928 0.261 ± 0.042	$\begin{array}{c} 0.896 \pm 0.000 \\ 0.725 \pm 0.002 \\ 0.474 \pm 0.202 \end{array}$	$\begin{array}{c} 0.729 \pm 0.019 \\ \underline{0.816 \pm 0.168} \\ 0.575 \pm 0.054 \end{array}$	7.8 5.8 8.3
Gradient Ascent COMs BONET	$\begin{array}{c} 0.981 \pm 0.015 \\ \hline 0.964 \pm 0.020 \\ 0.975 \pm 0.004 \end{array}$	0.659 ± 0.039 0.654 ± 0.020 0.681 ± 0.035	$\begin{array}{c} 0.647 \pm 0.020 \\ 0.648 \pm 0.005 \\ \underline{0.654 \pm 0.019} \end{array}$	0.504 ± 0.005 0.423 ± 0.033 0.437 ± 0.022	0.340 ± 0.034 0.949 ± 0.021 0.976 ± 0.012	$\begin{array}{c} 0.906 \pm 0.017 \\ 0.948 \pm 0.006 \\ \underline{0.954 \pm 0.012} \end{array}$	$\begin{array}{c} 0.672 \pm 0.021 \\ 0.764 \pm 0.018 \\ 0.780 \pm 0.022 \end{array}$	5.0 5.8 <u>3.7</u>
CbAS MINs DDOM Ours	0.958 ± 0.018 0.938 ± 0.047 0.971 ± 0.005 0.990 ± 0.003	$\begin{array}{c} 0.657 \pm 0.017 \\ 0.659 \pm 0.044 \\ 0.688 \pm 0.092 \\ \hline 0.803 \pm 0.085 \end{array}$	$\begin{array}{c} 0.640 \pm 0.005 \\ 0.653 \pm 0.002 \\ 0.633 \pm 0.007 \\ \textbf{0.661} \pm \textbf{0.025} \end{array}$	$\begin{array}{c} 0.450 \pm 0.083 \\ 0.484 \pm 0.017 \\ \underline{0.560 \pm 0.044} \\ \mathbf{0.567 \pm 0.017} \end{array}$	$\begin{array}{c} 0.876 \pm 0.015 \\ 0.942 \pm 0.018 \\ 0.957 \pm 0.012 \\ 0.982 \pm 0.012 \end{array}$	$\begin{array}{c} 0.896 \pm 0.016 \\ 0.944 \pm 0.009 \\ 0.926 \pm 0.009 \\ \textbf{0.961} \pm \textbf{0.006} \end{array}$	0.746 ± 0.003 0.770 ± 0.023 0.787 ± 0.034 0.827 ± 0.021	7.3 5.5 4.5 1.2

Main results We observe in Tabs. 2 and 3 that LEO achieves the best average rank of 1.2 and 1.8 among all the baselines with Q of 256 and 128, where the runner-up is BONET [19] and Tri-mentoring [22] with the average rank of 3.7 and 2.8. LEO consistently achieves the best normalized mean values across all tasks in these set-ups, outperforming all the baselines particularly the generative-model-based inverse approaches [10, 11]; this confirms the effectiveness of our model design. Specifically, for Q = 256 we report the best result on all 6 sub-tasks except **ANT**. We note that the best-performing baseline on this task, CMA-ES, has a std. of 0.928 which is significantly larger than ours, 0.012; this indicates its undesirable sensitivity to initialization. For Q = 128 we report the best results on 3 out

²NAS and Hopper tasks are excluded (see Appx. E.2.2).

of 5 sub-tasks. ExPT [20] focuses extensively on few-shot learning scenarios with models pre-trained on larger datasets, and are therefore not directly comparable to other baseline methods. We observe that our method demonstrates top-tier if not the best performances on the remaining two sub-tasks.

Table 3: Normalized design-bench results with Q=128. Baseline numbers from [12, 18, 20, 22]. ChEMBL dataset is excluded following baseline set-ups. * indicates that the baseline has slightly different set-ups; the numbers are for rough reference (see Appx. E.2.3 for more details).

BASELINE	TFBIND8	TFBIND10	SUPERCON.	ANT	D'KITTY	MEAN SCORE [↑]	$\mathbf{MNR}^{\downarrow}$
D (best)	0.439	0.467	0.399	0.565	0.884	-	-
GP-qEI	0.798 ± 0.083	0.652 ± 0.038	0.402 ± 0.034	0.819 ± 0.000	0.896 ± 0.000	0.713	14.2
CMA-ES	0.953 ± 0.022	0.670 ± 0.023	0.465 ± 0.024	$\bf 1.214 \pm 0.732$	0.724 ± 0.001	0.805	8.6
REINFORCE	0.948 ± 0.028	0.663 ± 0.034	0.481 ± 0.013	0.266 ± 0.032	0.562 ± 0.196	0.584	12.4
*BOOTGEN	0.979 ± 0.001	-	-	-	-	-	-
*ExPT	0.933 ± 0.036	0.677 ± 0.048	-	0.970 ± 0.004	0.973 ± 0.005	-	-
Grad. Ascent	0.886 ± 0.035	0.647 ± 0.021	0.495 ± 0.011	0.934 ± 0.011	0.944 ± 0.017	0.781	10.2
COMS	0.496 ± 0.065	0.622 ± 0.003	0.491 ± 0.028	0.856 ± 0.040	0.938 ± 0.015	0.681	13.4
BONET	0.911 ± 0.005	0.756 ± 0.006	0.500 ± 0.002	0.927 ± 0.002	0.954 ± 0.000	0.810	6.8
ROMA	0.924 ± 0.040	0.666 ± 0.035	0.510 ± 0.015	0.917 ± 0.030	0.927 ± 0.013	0.789	8.2
NEMO	0.943 ± 0.005	0.711 ± 0.021	0.502 ± 0.002	0.958 ± 0.011	0.954 ± 0.007	0.814	5.2
BDI	0.870 ± 0.000	0.605 ± 0.000	0.513 ± 0.000	0.906 ± 0.000	0.919 ± 0.000	0.763	11.6
IOM	0.878 ± 0.069	0.648 ± 0.023	0.520 ± 0.018	0.918 ± 0.031	0.945 ± 0.012	0.782	8.6
ICT	0.958 ± 0.008	0.691 ± 0.023	0.503 ± 0.017	0.961 ± 0.007	0.968 ± 0.020	0.816	3.4
Tri-mtring	0.970 ± 0.001	0.722 ± 0.017	0.514 ± 0.018	0.948 ± 0.014	0.966 ± 0.010	0.824	3
CbAS	0.927 ± 0.051	0.651 ± 0.060	0.503 ± 0.069	0.876 ± 0.031	0.892 ± 0.008	0.770	10.8
Auto.CbAS	0.910 ± 0.044	0.630 ± 0.045	0.421 ± 0.045	0.882 ± 0.045	0.906 ± 0.006	0.745	13
MINs	0.905 ± 0.052	0.616 ± 0.021	0.499 ± 0.017	0.445 ± 0.080	0.892 ± 0.011	0.671	13.6
DDOM	0.957 ± 0.006	0.657 ± 0.006	0.495 ± 0.012	0.940 ± 0.004	0.935 ± 0.001	0.797	8
Ours	0.983 ± 0.011	0.771 ± 0.096	0.559 ± 0.024	0.954 ± 0.008	0.954 ± 0.004	0.844	2

4.3 Ablation Study

In this section, we would like to inspect: i) the impact of important hyperparameters for LEO, ii) the impact of NTRE compared with MLE on learning the LEBM $p_{\alpha}(\mathbf{z})$, iii) whether an energy-based latent space model is necessary, and iv) impact of different sampling techniques. We again use the design-bench suite for the ablative experiments to empirically answer these questions.

Table 4: **Ablation studies on design-bench with** Q = 256. Results sampled with SVGD by default.

BASELINE	TFBIND8	TFBIND10	CHEMBL	SUPERCON.	ANT	D'KITTY	MEAN SCORE [↑]
\mathcal{D} (best)	0.439	0.467	0.399	0.565	0.884	0.605	-
Gaussian w/ LD MLE-LEBM w/ LD Ours w/ LD	0.909 ± 0.077 0.524 ± 0.228 0.834 ± 0.073	0.659 ± 0.012 0.667 ± 0.000 0.739 ± 0.095	0.652 ± 0.012 0.633 ± 0.000 0.639 ± 0.013	0.406 ± 0.022 0.362 ± 0.006 0.363 ± 0.006	$\begin{array}{c} 0.948 \pm 0.016 \\ 0.512 \pm 0.000 \\ \underline{0.957 \pm 0.023} \end{array}$	0.933 ± 0.006 0.672 ± 0.049 0.955 ± 0.004	$\begin{array}{c} 0.751 \pm 0.010 \\ 0.562 \pm 0.033 \\ 0.748 \pm 0.025 \end{array}$
Gaussian w/ SVGD MLE-LEBM w/ SVGD	$\begin{array}{c} 0.923 \pm 0.071 \\ 0.941 \pm 0.012 \end{array}$	$\begin{array}{c} 0.669 \pm 0.010 \\ 0.681 \pm 0.079 \end{array}$	$\begin{array}{c} 0.650 \pm 0.001 \\ \hline 0.634 \pm 0.002 \end{array}$	0.403 ± 0.021 0.296 ± 0.004	$\begin{array}{c} 0.942 \pm 0.006 \\ 0.926 \pm 0.016 \end{array}$	$\begin{array}{c} 0.933 \pm 0.004 \\ 0.915 \pm 0.007 \end{array}$	0.753 ± 0.010 0.732 ± 0.014
Ours w/ $K+1=1, M=100$ Ours w/ $K+1=6, M=1$ Ours	$\begin{array}{c} 0.945 \pm 0.025 \\ \underline{0.961 \pm 0.024} \\ \mathbf{0.990 \pm 0.003} \end{array}$	0.722 ± 0.043 0.655 ± 0.034 0.803 ± 0.085	$\begin{array}{c} 0.648 \pm 0.003 \\ 0.640 \pm 0.011 \\ \textbf{0.661} \pm \textbf{0.025} \end{array}$	$0.421 \pm 0.020 \\ \underline{0.497 \pm 0.044} \\ \mathbf{0.567 \pm 0.017}$	0.893 ± 0.008 0.907 ± 0.007 0.982 ± 0.012	$\begin{array}{c} 0.953 \pm 0.008 \\ \underline{0.959 \pm 0.002} \\ \mathbf{0.961 \pm 0.006} \end{array}$	0.764 ± 0.005 0.770 ± 0.007 0.827 ± 0.021

We term the inverse model parameterized by a MLE-learned p_{α} as MLE-LEBM, and the model parameterized by a non-informative Gaussian prior as Gaussian in Tab. 4. We present results of these variants and our model obtained by both LD [56] and SVGD [64] samplers. We can see that our model learned by Eq. (9) produces decent results compared with other variants, validating our design choices. We provide ablative results on noise intensity

Table 5: Ablation of K, M on SUPERCON.

M = 100	K + 1 = 2	K + 1 = 4	K + 1 = 6	K+1=8
M = 100	0.427 ± 0.013	$0.557{\pm}0.029$	0.567 ± 0.017	0.527 ± 0.049
K+1=6	M = 1	M = 10	M = 100	M = 1000
K+1=0	0.497±0.044	0.486 ± 0.023	0.567±0.017	0.548±0.046

Table 6: **Ablation of** *Q* **on D'Kitty.**

Q = 2	Q = 8	Q = 32	Q = 128	Q = 256
0.906 ± 0.009	$0.925{\pm}0.013$	$0.937{\pm}0.006$	$0.954 {\pm} 0.004$	0.961 ± 0.006

M, number of intermediate stages K+1 and query budget Q in Tabs. 4 to 6. Of note, K+1=1 means learning a LEBM w/ Eq. (9) alone, w/o ratio decomposition; M=1 means learning with the original TRE objective, w/o intensifying the noise distributions. These results further confirm our assumptions about the noise intensity, demonstrate the need for ratio decomposition and show that LEO is robust to Q. We refer to Appx. E.2.4 for extended and more in-depth discussions.

5 Conclusion

In this paper, we introduce a novel framework LEO, backed by i) an energy-based latent space induced with an MCMC-free learning scheme and ii) an expanding-exploration model design for solving the offline BBO problem. We provide theoretical and empirical evidence for the effectiveness of our approach; we discuss limitations and potential impacts in Appx. F.1 and F.2.

References

- [1] David Brookes, Hahnbeom Park, and Jennifer Listgarten. Conditioning by adaptive sampling for robust design. In *International conference on machine learning*, pages 773–782. PMLR, 2019. 1, 2, 8, A1, A10
- [2] Dinghuai Zhang, Jie Fu, Yoshua Bengio, and Aaron C. Courville. Unifying likelihood-free inference with black-box optimization and beyond. In *International Conference on Learning Representations (ICLR)*, 2021. 1
- [3] Anna Gaulton, Louisa J Bellis, A Patricia Bento, Jon Chambers, Mark Davies, Anne Hersey, Yvonne Light, Shaun McGlinchey, David Michalovich, Bissan Al-Lazikani, et al. Chembl: a large-scale bioactivity database for drug discovery. *Nucleic acids research*, 40(D1):D1100– D1107, 2012. 1
- [4] Deqian Kong, Yuhao Huang, Jianwen Xie, and Ying Nian Wu. Molecule design by latent prompt transformer. *arXiv preprint arXiv:2310.03253*, 2023. 3, A1
- [5] Deqian Kong, Bo Pang, Tian Han, and Ying Nian Wu. Molecule design by latent space energy-based modeling and gradual distribution shifting. In *Uncertainty in Artificial Intelligence*, pages 1109–1120. PMLR, 2023. 1, 3, A1
- [6] Felix Berkenkamp, Angela P Schoellig, and Andreas Krause. Safe controller optimization for quadrotors with gaussian processes. In 2016 IEEE international conference on robotics and automation (ICRA), pages 491–496. IEEE, 2016. 1
- [7] Bobak Shahriari, Kevin Swersky, Ziyu Wang, Ryan P Adams, and Nando De Freitas. Taking the human out of the loop: A review of bayesian optimization. *Proceedings of the IEEE*, 104 (1):148–175, 2015. 2, 3, A1
- [8] Jeffrey Larson, Matt Menickelly, and Stefan M Wild. Derivative-free optimization methods. *Acta Numerica*, 28:287–404, 2019. 2
- [9] Clara Fannjiang and Jennifer Listgarten. Autofocused oracles for model-based design. *Advances in Neural Information Processing Systems*, 33:12945–12956, 2020. 2, 8, A1, A10
- [10] Aviral Kumar and Sergey Levine. Model inversion networks for model-based optimization. Advances in Neural Information Processing Systems, 33:5126–5137, 2020. 2, 3, 6, 8, A1, A7, A10
- [11] Siddarth Krishnamoorthy, Satvik Mehul Mashkaria, and Aditya Grover. Diffusion models for black-box optimization. In *International Conference on Machine Learning*, 2023. 2, 3, 5, 6, 7, 8, A1, A7, A9, A10, A11, A14
- [12] Minsu Kim, Federico Berto, Sungsoo Ahn, and Jinkyoo Park. Bootstrapped training of score-conditioned generator for offline design of biological sequences. *Advances in Neural Information Processing Systems*, 36, 2024. 2, 9, A1, A11, A12
- [13] Justin Fu and Sergey Levine. Offline model-based optimization via normalized maximum likelihood estimation. In *International Conference on Learning Representations*, 2020. 2, 8, A1, A10
- [14] Sihyun Yu, Sungsoo Ahn, Le Song, and Jinwoo Shin. Roma: Robust model adaptation for offline model-based optimization. *Advances in Neural Information Processing Systems*, 34: 4619–4631, 2021. 8, A1, A10
- [15] Brandon Trabucco, Aviral Kumar, Xinyang Geng, and Sergey Levine. Conservative objective models for effective offline model-based optimization. In *International Conference on Machine Learning*, pages 10358–10368. PMLR, 2021. A1, A7, A10
- [16] Can Chen, Yingxueff Zhang, Jie Fu, Xue Steve Liu, and Mark Coates. Bidirectional learning for offline infinite-width model-based optimization. *Advances in Neural Information Processing Systems*, 35:29454–29467, 2022. 2, A10

- [17] Han Qi, Yi Su, Aviral Kumar, and Sergey Levine. Data-driven offline decision-making via invariant representation learning. Advances in Neural Information Processing Systems, 35: 13226–13237, 2022. A10
- [18] Ye Yuan, Can Sam Chen, Zixuan Liu, Willie Neiswanger, and Xue Steve Liu. Importance-aware co-teaching for offline model-based optimization. *Advances in Neural Information Processing Systems*, 36, 2024. 2, 8, 9, A1, A9, A10, A12
- [19] Satvik Mehul Mashkaria, Siddarth Krishnamoorthy, and Aditya Grover. Generative pretraining for black-box optimization. In *International Conference on Machine Learning*, pages 24173– 24197. PMLR, 2023. 2, 7, 8, A1, A7, A9, A10, A11, A13
- [20] Tung Nguyen, Sudhanshu Agrawal, and Aditya Grover. Expt: Synthetic pretraining for few-shot experimental design. Advances in Neural Information Processing Systems, 36, 2024. 2, 9, A11, A12
- [21] Brandon Trabucco, Xinyang Geng, Aviral Kumar, and Sergey Levine. Design-bench: Benchmarks for data-driven offline model-based optimization. In *International Conference on Machine Learning*, pages 21658–21676. PMLR, 2022. 2, 3, 8, A1, A9, A10
- [22] Can Sam Chen, Christopher Beckham, Zixuan Liu, Xue Steve Liu, and Chris Pal. Parallel-mentoring for offline model-based optimization. *Advances in Neural Information Processing Systems*, 36, 2024. 2, 8, 9, A1, A10, A12
- [23] R Garnett, M Osborne, and P Hennig. Active learning of linear embeddings for gaussian processes. In *30th Conference on Uncertainty in Artificial Intelligence (UAI 2014)*, pages 230–239. AUAI Press, 2014. 2, A1
- [24] Santu Rana, Cheng Li, Sunil Gupta, Vu Nguyen, and Svetha Venkatesh. High dimensional bayesian optimization with elastic gaussian process. In *International conference on machine learning*, pages 2883–2891. PMLR, 2017.
- [25] Riccardo Moriconi, Marc Peter Deisenroth, and KS Sesh Kumar. High-dimensional bayesian optimization using low-dimensional feature spaces. *Machine Learning*, 109:1925–1943, 2020. 2, A1
- [26] James T Wilson, Riccardo Moriconi, Frank Hutter, and Marc Peter Deisenroth. The reparameterization trick for acquisition functions. arXiv preprint arXiv:1712.00424, 2017. 2, A10
- [27] Bo Pang, Tian Han, Erik Nijkamp, Song-Chun Zhu, and Ying Nian Wu. Learning latent space energy-based prior model. In Advances in Neural Information Processing Systems (NeurIPS), 2020. 2, 3, 4, A1
- [28] Peiyu Yu, Yongming Rao, Jiwen Lu, and Jie Zhou. P2gnet: Pose-guided point cloud generating networks for 6-dof object pose estimation. *arXiv preprint arXiv:1912.09316*, 2019.
- [29] Peiyu Yu, Sirui Xie, Xiaojian Ma, Yixin Zhu, Ying Nian Wu, and Song-Chun Zhu. Unsupervised foreground extraction via deep region competition. Advances in Neural Information Processing Systems, 34:14264–14279, 2021. 3, A1
- [30] Peiyu Yu, Sirui Xie, Xiaojian Ma, Baoxiong Jia, Bo Pang, Ruiqi Gao, Yixin Zhu, Song-Chun Zhu, and Ying Nian Wu. Latent diffusion energy-based model for interpretable text modeling. arXiv preprint arXiv:2206.05895, 2022. 3, 4, 6, A1, A8
- [31] Peiyu Yu, Yaxuan Zhu, Sirui Xie, Xiaojian Shawn Ma, Ruiqi Gao, Song-Chun Zhu, and Ying Nian Wu. Learning energy-based prior model with diffusion-amortized mcmc. Advances in Neural Information Processing Systems, 36, 2024. A14
- [32] Yasi Zhang, Peiyu Yu, and Ying Nian Wu. Object-conditioned energy-based attention map alignment in text-to-image diffusion models. *arXiv preprint arXiv:2404.07389*, 2024.
- [33] Yilue Qian, Peiyu Yu, Ying Nian Wu, Wei Wang, and Lifeng Fan. Learning concept-based visual causal transition and symbolic reasoning for visual planning. *arXiv* preprint *arXiv*:2310.03325, 2023.

- [34] Jianwen Xie, Yaxuan Zhu, Yifei Xu, Dingcheng Li, and Ping Li. A tale of two latent flows: Learning latent space normalizing flow with short-run langevin flow for approximate inference. In *Thirty-Seventh AAAI Conference on Artificial Intelligence*, pages 10499–10509, 2023.
- [35] Yaxuan Zhu, Jianwen Xie, and Ping Li. Likelihood-based generative radiance field with latent space energy-based model for 3d-aware disentangled image representation. In *International Conference on Artificial Intelligence and Statistics*, volume 206, pages 4164–4180, 2023.
- [36] Joseph Cho, Fachrina Dewi Puspitasari, Sheng Zheng, Jingyao Zheng, Lik-Hang Lee, Tae-Ho Kim, Choong Seon Hong, and Chaoning Zhang. Sora as an agi world model? a complete survey on text-to-video generation. *arXiv* preprint arXiv:2403.05131, 2024.
- [37] Yingshan Chang, Yasi Zhang, Zhiyuan Fang, Yingnian Wu, Yonatan Bisk, and Feng Gao. Skews in the phenomenon space hinder generalization in text-to-image generation, 2024.
- [38] Hengzhi He, Peiyu Yu, Junpeng Ren, Ying Nian Wu, and Guang Cheng. Watermarking generative tabular data. *arXiv preprint arXiv:2405.14018*, 2024. 2
- [39] Riccardo Moriconi, KS Sesh Kumar, and Marc Peter Deisenroth. High-dimensional bayesian optimization with projections using quantile gaussian processes. *Optimization Letters*, 14: 51–64, 2020. 2, A1
- [40] Kirthevasan Kandasamy, Jeff Schneider, and Barnabás Póczos. High dimensional bayesian optimisation and bandits via additive models. In *International conference on machine learning*, pages 295–304. PMLR, 2015.
- [41] Paul Rolland, Jonathan Scarlett, Ilija Bogunovic, and Volkan Cevher. High-dimensional bayesian optimization via additive models with overlapping groups. In *International conference on artificial intelligence and statistics*, pages 298–307. PMLR, 2018. 2
- [42] Nando de Freitas and Ziyu Wang. Bayesian optimization in high dimensions via random embeddings. 2013. 2
- [43] Matt J Kusner, Brooks Paige, and José Miguel Hernández-Lobato. Grammar variational autoencoder. In *International conference on machine learning*, pages 1945–1954. PMLR, 2017.
- [44] Xiaoyu Lu, Javier Gonzalez, Zhenwen Dai, and Neil D Lawrence. Structured variationally autoencoded optimization. In *International conference on machine learning*, pages 3267–3275. PMLR, 2018.
- [45] Rafael Gómez-Bombarelli, Jennifer N Wei, David Duvenaud, José Miguel Hernández-Lobato, Benjamín Sánchez-Lengeling, Dennis Sheberla, Jorge Aguilera-Iparraguirre, Timothy D Hirzel, Ryan P Adams, and Alán Aspuru-Guzik. Automatic chemical design using a data-driven continuous representation of molecules. *ACS central science*, 4(2):268–276, 2018. 2, A1
- [46] Diederik P Kingma and Max Welling. Auto-encoding variational bayes. *arXiv preprint* arXiv:1312.6114, 2013. 2, 3
- [47] Danilo Jimenez Rezende, Shakir Mohamed, and Daan Wierstra. Stochastic backpropagation and approximate inference in deep generative models. In *International Conference on Machine Learning (ICML)*, 2014. 2, A1
- [48] Ruiqi Gao, Yang Song, Ben Poole, Ying Nian Wu, and Diederik P Kingma. Learning energy-based models by diffusion recovery likelihood. In *International Conference on Learning Representations (ICLR)*, 2020. 3, A1
- [49] Jianwen Xie, Yang Lu, Song-Chun Zhu, and Yingnian Wu. A theory of generative convnet. In *International Conference on Machine Learning*, pages 2635–2644, 2016. 3, 4, A1
- [50] Jianwen Xie, Yang Lu, Ruiqi Gao, Song-Chun Zhu, and Ying Nian Wu. Cooperative training of descriptor and generator networks. *IEEE Trans. Pattern Anal. Mach. Intell.*, 42(1):27–45, 2020.

- [51] Will Grathwohl, Kuan-Chieh Wang, Joern-Henrik Jacobsen, David Duvenaud, Mohammad Norouzi, and Kevin Swersky. Your classifier is secretly an energy based model and you should treat it like one. In *International Conference on Learning Representations (ICLR)*, 2019.
- [52] Erik Nijkamp, Mitch Hill, Song-Chun Zhu, and Ying Nian Wu. Learning non-convergent non-persistent short-run mcmc toward energy-based model. In *Advances in Neural Information Processing Systems (NeurIPS)*, 2019. A1
- [53] Erik Nijkamp, Mitch Hill, Tian Han, Song-Chun Zhu, and Ying Nian Wu. On the anatomy of mcmc-based maximum likelihood learning of energy-based models. In *AAAI Conference on Artificial Intelligence (AAAI)*, 2020. 3, A1
- [54] Benjamin Rhodes, Kai Xu, and Michael U Gutmann. Telescoping density-ratio estimation. *Advances in neural information processing systems*, 33:4905–4916, 2020. 3, 4, A1
- [55] Jasper Snoek, Hugo Larochelle, and Ryan P Adams. Practical bayesian optimization of machine learning algorithms. Advances in neural information processing systems, 25, 2012. 3, A1
- [56] Max Welling and Yee W Teh. Bayesian learning via stochastic gradient langevin dynamics. In International Conference on Machine Learning (ICML), 2011. 4, 9
- [57] Trevor Hastie, Robert Tibshirani, Jerome H Friedman, and Jerome H Friedman. The elements of statistical learning: data mining, inference, and prediction, volume 2. Springer, 2009. 4, A1
- [58] Masashi Sugiyama, Taiji Suzuki, and Takafumi Kanamori. *Density ratio estimation in machine learning*. Cambridge University Press, 2012.
- [59] Michael U Gutmann and Aapo Hyvärinen. Noise-contrastive estimation of unnormalized statistical models, with applications to natural image statistics. *Journal of machine learning research*, 13(2), 2012. 4, 7, A1
- [60] Michael Gutmann and Aapo Hyvärinen. Noise-contrastive estimation: A new estimation principle for unnormalized statistical models. In *International Conference on Artificial Intelligence and Statistics (AISTATS)*, pages 297–304. JMLR Workshop and Conference Proceedings, 2010.
- [61] Miika Pihlaja, Michael Gutmann, and Aapo Hyvärinen. A family of computationally efficient and simple estimators for unnormalized statistical models. In *Proceedings of the Twenty-Sixth Conference on Uncertainty in Artificial Intelligence*, pages 442–449, 2010.
- [62] Aditya Menon and Cheng Soon Ong. Linking losses for density ratio and class-probability estimation. In *International Conference on Machine Learning*, pages 304–313. PMLR, 2016.
- [63] Ben Poole, Sherjil Ozair, Aaron Van Den Oord, Alex Alemi, and George Tucker. On variational bounds of mutual information. In *International Conference on Machine Learning*, pages 5171– 5180. PMLR, 2019. 4
- [64] Qiang Liu and Dilin Wang. Stein variational gradient descent: A general purpose bayesian inference algorithm. *Advances in neural information processing systems*, 29, 2016. 4, 9, A9
- [65] Jakub Tomczak and Max Welling. Vae with a vampprior. In *International Conference on Artificial Intelligence and Statistics*, pages 1214–1223. PMLR, 2018. 5
- [66] A Mnih and Y Teh. A fast and simple algorithm for training neural probabilistic language models. In *International Conference on Machine Learning (ICML)*, volume 2, 2012. 5, A8
- [67] Jonathan Ho, Ajay Jain, and Pieter Abbeel. Denoising diffusion probabilistic models. In *Advances in Neural Information Processing Systems (NeurIPS)*, 2020. 6, A1, A8, A10
- [68] Bingbin Liu, Elan Rosenfeld, Pradeep Kumar Ravikumar, and Andrej Risteski. Analyzing and improving the optimization landscape of noise-contrastive estimation. In *International Conference on Learning Representations*, 2021. 7, A5, A6

- [69] Ting Chen, Simon Kornblith, Mohammad Norouzi, and Geoffrey Hinton. A simple framework for contrastive learning of visual representations. In *International conference on machine learning*, pages 1597–1607. PMLR, 2020. 7
- [70] Niranjan Srinivas, Andreas Krause, Sham Kakade, and Matthias Seeger. Gaussian process optimization in the bandit setting: no regret and experimental design. In *Proceedings of the 27th International Conference on International Conference on Machine Learning*, pages 1015–1022, 2010. A1
- [71] Vu Nguyen and Michael A Osborne. Knowing the what but not the where in bayesian optimization. In *International Conference on Machine Learning*, pages 7317–7326. PMLR, 2020. A1
- [72] Reuven Y Rubinstein and Dirk P Kroese. *The cross-entropy method: a unified approach to combinatorial optimization, Monte-Carlo simulation, and machine learning*, volume 133. Springer, 2004. A1
- [73] Ronald J Williams. Simple statistical gradient-following algorithms for connectionist reinforcement learning. *Machine learning*, 8:229–256, 1992. A1, A10
- [74] Reuven Y Rubinstein. Optimization of computer simulation models with rare events. *European Journal of Operational Research*, 99(1):89–112, 1997. A1
- [75] Jan Peters and Stefan Schaal. Reinforcement learning by reward-weighted regression for operational space control. In *Proceedings of the 24th international conference on Machine learning*, pages 745–750, 2007. A1
- [76] Jasper Snoek, Oren Rippel, Kevin Swersky, Ryan Kiros, Nadathur Satish, Narayanan Sundaram, Mostofa Patwary, Mr Prabhat, and Ryan Adams. Scalable bayesian optimization using deep neural networks. In *International conference on machine learning*, pages 2171–2180. PMLR, 2015. A1
- [77] Hyunjik Kim, Andriy Mnih, Jonathan Schwarz, Marta Garnelo, Ali Eslami, Dan Rosenbaum, Oriol Vinyals, and Yee Whye Teh. Attentive neural processes. In *International Conference on Learning Representations*, 2018. A1
- [78] Marta Garnelo, Dan Rosenbaum, Christopher Maddison, Tiago Ramalho, David Saxton, Murray Shanahan, Yee Whye Teh, Danilo Rezende, and SM Ali Eslami. Conditional neural processes. In *International conference on machine learning*, pages 1704–1713. PMLR, 2018.
- [79] Marta Garnelo, Jonathan Schwarz, Dan Rosenbaum, Fabio Viola, Danilo J Rezende, SM Eslami, and Yee Whye Teh. Neural processes. *arXiv preprint arXiv:1807.01622*, 2018. A1
- [80] Christof Angermueller, David Dohan, David Belanger, Ramya Deshpande, Kevin Murphy, and Lucy Colwell. Model-based reinforcement learning for biological sequence design. In *International conference on learning representations*, 2019. A1
- [81] Christof Angermueller, David Belanger, Andreea Gane, Zelda Mariet, David Dohan, Kevin Murphy, Lucy Colwell, and D Sculley. Population-based black-box optimization for biological sequence design. In *International Conference on Machine Learning*, pages 324–334. PMLR, 2020.
- [82] Azalia Mirhoseini, Anna Goldie, Mustafa Yazgan, Joe Jiang, Ebrahim Songhori, Shen Wang, Young-Joon Lee, Eric Johnson, Omkar Pathak, Sungmin Bae, et al. Chip placement with deep reinforcement learning. *arXiv preprint arXiv:2004.10746*, 2020. A1
- [83] Ian Goodfellow, Jean Pouget-Abadie, Mehdi Mirza, Bing Xu, David Warde-Farley, Sherjil Ozair, Aaron Courville, and Yoshua Bengio. Generative adversarial networks. *Communications of the ACM*, 63(11):139–144, 2020. A1, A10
- [84] Mehdi Mirza and Simon Osindero. Conditional generative adversarial nets. arXiv preprint arXiv:1411.1784, 2014. A1, A10

- [85] Yilun Du and Igor Mordatch. Implicit generation and generalization in energy-based models. *arXiv preprint arXiv:1903.08689*, 2019. A1
- [86] Yilun Du, Shuang Li, Joshua Tenenbaum, and Igor Mordatch. Improved contrastive divergence training of energy based models. In *International Conference on Machine Learning (ICML)*, 2021. A1
- [87] Bo Pang, Tian Han, and Ying Nian Wu. Learning latent space energy-based prior model for molecule generation. arXiv preprint arXiv:2010.09351, 2020. A1
- [88] Bo Pang, Tianyang Zhao, Xu Xie, and Ying Nian Wu. Trajectory prediction with latent belief energy-based model. In Conference on Computer Vision and Pattern Recognition (CVPR), 2021. A1
- [89] Zhuowen Tu. Learning generative models via discriminative approaches. In 2007 IEEE Conference on Computer Vision and Pattern Recognition, pages 1–8. IEEE, 2007. A1
- [90] Justin Lazarow, Long Jin, and Zhuowen Tu. Introspective neural networks for generative modeling. In *Proceedings of the IEEE International Conference on Computer Vision*, pages 2774–2783, 2017.
- [91] Ciwan Ceylan and Michael U Gutmann. Conditional noise-contrastive estimation of unnormalised models. In *International Conference on Machine Learning*, pages 726–734. PMLR, 2018.
- [92] Aditya Grover and Stefano Ermon. Boosted generative models. In *Proceedings of the AAAI Conference on Artificial Intelligence*, volume 32, 2018.
- [93] Ruiqi Gao, Erik Nijkamp, Diederik P Kingma, Zhen Xu, Andrew M Dai, and Ying Nian Wu. Flow contrastive estimation of energy-based models. In *Proceedings of the IEEE/CVF Conference on Computer Vision and Pattern Recognition*, pages 7518–7528, 2020. A1
- [94] Jyoti Aneja, Alex Schwing, Jan Kautz, and Arash Vahdat. A contrastive learning approach for training variational autoencoder priors. Advances in neural information processing systems, 34:480–493, 2021. A1
- [95] Durk P Kingma and Prafulla Dhariwal. Glow: Generative flow with invertible 1x1 convolutions. *Advances in neural information processing systems*, 31, 2018. A1
- [96] Zhisheng Xiao and Tian Han. Adaptive multi-stage density ratio estimation for learning latent space energy-based model. *Advances in Neural Information Processing Systems (NeurIPS)*, 2022. A2
- [97] Geoffrey E Hinton, Simon Osindero, and Yee-Whye Teh. A fast learning algorithm for deep belief nets. *Neural computation*, 18(7):1527–1554, 2006. A5
- [98] Andrew Brock, Theodore Lim, James M Ritchie, and Nick Weston. Neural photo editing with introspective adversarial networks. *arXiv preprint arXiv:1609.07093*, 2016. A8
- [99] Adam Paszke, Sam Gross, Francisco Massa, Adam Lerer, James Bradbury, Gregory Chanan, Trevor Killeen, Zeming Lin, Natalia Gimelshein, Luca Antiga, et al. Pytorch: An imperative style, high-performance deep learning library. In *Advances in Neural Information Processing Systems (NeurIPS)*, 2019. A8
- [100] Diederik P Kingma and Jimmy Ba. Adam: A method for stochastic optimization. *arXiv* preprint arXiv:1412.6980, 2014. A8, A9
- [101] John Duchi, Elad Hazan, and Yoram Singer. Adaptive subgradient methods for online learning and stochastic optimization. *Journal of machine learning research*, 12(7), 2011. A9
- [102] Nikolaus Hansen. The cma evolution strategy: a comparing review. *Towards a new evolutionary computation: Advances in the estimation of distribution algorithms*, pages 75–102, 2006. A10
- [103] Jiaxin Shi and Lester Mackey. A finite-particle convergence rate for stein variational gradient descent. Advances in Neural Information Processing Systems, 36, 2024. A14

A Related Work

Online BBO An important set-up for BBO problems is the online BBO, also referred to as active BBO in many literature [4, 5, 11, 19]. For online BBO, the proposed method can query the black-box function with limited times during training. A probably most well-known family is BO, with a large body of prior work in the area [7, 23, 25, 39–45, 55, 70, 71]. Typically, BO employs surrogates such as Gaussian Processes to model the underlying function, where the surrogates are sequentially updated by querying the black-box function with newly proposed points from an uncertainty-aware acquisition function. Other branches include derivative free methods such as the cross-entropy method [72], methods derived from the REINFORCE trick [73, 74] and reward-weighted regression [75], etc. Several practical approaches have combined these methodologies with Bayesian neural networks [55, 76], neural processes [77–79], and ensembles of learned score models [80–82] with extensive efforts in developing advanced querying mechanisms or better approximation of the surrogates to address the online BBO problem.

Offline BBO Recent works have shown significant progress in the offline BBO set-up [1, 9–12, 14– 19, 21, 22, 13]. Among them, [10] trains a stochastic inverse mapping $p_{\theta}(\mathbf{x}|y) \propto \mathbb{E}_{p(\mathbf{z}|y)}[p(\mathbf{x}|\mathbf{z},y)]$ with a conditional GAN-like model to instantiate $p(\mathbf{x}|\mathbf{z},y)$ [83, 84]. The method optimizes over \mathbf{z} given the offline dataset maximum y_{max} and map z back to x for BBO solutions. The optimization process over z draw approximate samples from $p(\mathbf{z}|y)$. DDOM [11] consider directly parameterizing the inverse mapping $p_{\theta}(\mathbf{x}|y)$ with a conditional diffusion model in the input design space utilizing the expressiveness of DDPMs [67]. We show in Secs. 3.3 and 4.2 that our framework, LEO, backed by an accurately learned informative latent space and an expanding-exploration model design demonstrates significant improvements over previous parameterizations of inverse model. Forward methods [13, 15– 18, 22] employ gradient ascent to optimize the learned surrogates to propose candidate solutions for BBO. One critical issue, however, exists for the surrogate: the forward model can assign the out-oftraining-distribution input designs x with erroneously large values or underestimate the true support of the distribution [10, 19, 22], especially when the set of valid inputs lies in a low-dimensional manifold in the high-dimensional input design space. Several inspiring works have focus extensively on addressing this issue [14–18, 22]. For example, [14, 15] assign lower scores to identified outliers so that the approximated surrogate is expected to be robust. [19] instead mimic the optimization trajectories of black-box optimizers, and rolls out evaluation trajectories from the trained sequence model for optimization. Although the method circumvents the need of the surrogate, it assumes knowledge of the approximate value of the true optima during optimization, and can struggle relative to other approaches on certain domains. Our method learns an informative latent space suitable for BBO, and delivers strong results in comparison to prior works in Sec. 4.

Energy-based prior model As an interesting branch of Energy-Based Models (EBMs) [49, 52, 53, 85, 86], Pang et al. [27] show that an EBM can serve as an informative prior model in the latent space, *i.e.*, LEBM; such a prior greatly improves the model expressivity over those with non-informative gaussian priors and brings strong performance on downstream tasks [29, 30, 87, 88]. However, learning LEBM requires MCMC sampling to estimate the learning gradients, which needs careful tuning and numerous iterations to converge when the target distributions are high-dimensional or highly multimodal. Commonly-used short-run MCMC [52] in practice can lead to malformed energy landscapes and instability in training [30, 48, 53, 85, 86]. In this work, we consider inducing the informative latent space with NTRE integrated into variational learning; the proposed method requires no MCMC for estimating the prior model, and shows reliable sampling quality in practice.

Noise contrastive estimation Noise Contrastive Estimation (NCE) [57–59] provides a handy interface bridging the gap between discriminative and generative learning. An interesting line of research has been devoted to estimating unnormalized density, *i.e.*, EBMs or LEBMs, with NCE-like objectives [59, 89–94]. Particularly, Gao et al. [93] recruits a normalizing flow [47, 95] as the base distribution for density estimation. Aneja et al. [94] refine the prior distribution of a pre-trained powerful VAE with noise contrastive learning. However, plain NCE may fail in our set-up (see Tab. 4) as the target, *i.e.*, aggregated posterior can be far from the base Gaussian distribution. Rhodes et al. [54] identify this large ratio gap problem as *density-chasm*, and propose TRE to break the initial large ratio gap into several sub-problems with smaller gaps. We further propose the NTRE objective as a complement, and unveil the connection between maximum ELBO and Eq. (9) in variational learning. Tab. 4 confirms the effectiveness of NTRE over TRE in our set-up.

B Detailed Derivations and Proofs

B.1 Derivation of Eqs. (7) and (8)

Recall that the vanilla ELBO in Eq. (1) is

ELBO_{$$\boldsymbol{\theta}, \boldsymbol{\phi}$$} = log $p_{\boldsymbol{\theta}}(\mathbf{x}, y) - \mathbb{D}_{\mathrm{KL}}(q_{\boldsymbol{\phi}}(\mathbf{z}|\mathbf{x}, y)||p_{\boldsymbol{\theta}}(\mathbf{z}|\mathbf{x}, y))$
= $\mathbb{E}_{q_{\boldsymbol{\theta}}(\mathbf{z}|\mathbf{x}, y)}[\log p_{\boldsymbol{\beta}}(\mathbf{x}, y|\mathbf{z})] - \mathbb{D}_{\mathrm{KL}}(q_{\boldsymbol{\phi}}(\mathbf{z}|\mathbf{x}, y)||p_{\boldsymbol{\alpha}}(\mathbf{z})),$ (A1)

where \mathbb{D}_{KL} denotes the Kullback-Leibler divergence; $p_{\beta}(\mathbf{x}, y|\mathbf{z})$ denote the reconstruction of inputs and forward prediction model. In the definition of p_{α} :

$$p_{\alpha} = q_{K+1} = r_{\alpha_K} q_K$$

$$q_{k+1} = r_{\alpha_k} q_k = \frac{p_{\alpha_k}}{q_k} q_k, \ k = 0, ..., K.$$
(A2)

The implicitly learned distributions $p_{\alpha_0},...,p_{\alpha_K}$ in each ratio estimator r_{α_k} are designed to match the target distribution in each stage by minimizing the NTRE objective, i.e., $p_{\alpha_k} \approx q_{k+1}, k=0,...,K$, so that the telescoping product $\frac{q_{K+1}}{q_0} \approx \frac{p_{\alpha_K}}{q_K} \frac{p_{\alpha_{K-1}}}{q_{K-1}} \cdots \frac{p_{\alpha_0}}{q_0}$ holds as in Xiao and Han [96]. Specifically,

$$\log p_{\boldsymbol{\theta}}(\mathbf{x}, y) \ge \text{ELBO}_{\boldsymbol{\theta}, \boldsymbol{\phi}} = \log p_{\boldsymbol{\theta}}(\mathbf{x}, y) - \mathbb{D}_{\text{KL}}(q_{\boldsymbol{\phi}}(\mathbf{z}|\mathbf{x}, y) | p_{\boldsymbol{\theta}}(\mathbf{z}|\mathbf{x}, y))$$

$$= \mathbb{E}_{q_{\boldsymbol{\theta}}(\mathbf{z}|\mathbf{x}, y)}[\log p_{\boldsymbol{\beta}}(\mathbf{x}, y|\mathbf{z})] - \mathbb{D}_{\text{KL}}(q_{\boldsymbol{\phi}}(\mathbf{z}|\mathbf{x}, y) | p_{\boldsymbol{\alpha}}(\mathbf{z}))$$

$$= \mathbb{E}_{q_{\boldsymbol{\theta}}(\mathbf{z}|\mathbf{x}, y)}[\log p_{\boldsymbol{\beta}}(\mathbf{x}, y|\mathbf{z})] - \mathbb{D}_{\text{KL}}(q_{\boldsymbol{\phi}}(\mathbf{z}|\mathbf{x}, y) | r_{\boldsymbol{\alpha}_{K}} q_{K})$$

$$\ge \mathbb{E}_{q_{\boldsymbol{\phi}}}[\log p_{\boldsymbol{\beta}}(\mathbf{x}, y|\mathbf{z})] - \mathbb{D}_{\text{KL}}(q_{\boldsymbol{\phi}}(\mathbf{z}|\mathbf{x}, y) | r_{\boldsymbol{\alpha}_{K}}(\mathbf{z}) q_{K}(\mathbf{z}))$$

$$- \sum_{k=0}^{K-1} \mathbb{D}_{\text{KL}}(q_{k+1}(\mathbf{z}) | r_{\boldsymbol{\alpha}_{k}}(\mathbf{z}) q_{k}(\mathbf{z}))$$

$$= \text{ELBO}_{\text{re}} \boldsymbol{\theta}_{\boldsymbol{\phi}}.$$
(A3)

We can see that both $\mathrm{ELBO}_{\mathrm{re}, \pmb{\theta}, \pmb{\phi}}$ and $\mathrm{ELBO}_{\pmb{\theta}, \pmb{\phi}}$ are valid ELBOs of the observed data log-likelihood $\log p_{\pmb{\theta}}(\mathbf{x}, y)$, because $\mathbb{D}_{\mathrm{KL}} \geq 0$. We plug in $\sum_{k=0}^{K-1} \mathbb{D}_{\mathrm{KL}}(q_{k+1} \| r_{\pmb{\alpha}_k} q_k)$ to enforce $p_{\pmb{\alpha}_k} \approx q_{k+1}, k = 0, ..., K$ and obtain $\mathrm{ELBO}_{\mathrm{re}, \pmb{\theta}, \pmb{\phi}}$.

Taking the derivative of ELBO_{re, θ,ϕ} with regard to α_k , we can see that

$$\nabla_{\boldsymbol{\alpha}_{k}} \operatorname{ELBO}_{re} = \nabla_{\boldsymbol{\alpha}_{k}} \mathbb{D}_{\operatorname{KL}}(q_{k+1} \| r_{\boldsymbol{\alpha}_{k}} q_{k}) = \nabla_{\boldsymbol{\alpha}_{k}} \mathbb{D}_{\operatorname{KL}}(q_{k+1} \| p_{\boldsymbol{\alpha}_{k}})$$

$$= \nabla_{\boldsymbol{\alpha}_{k}} \mathbb{E}_{q_{k+1}} \left[\log p_{\boldsymbol{\alpha}_{k}} \right]$$

$$= \nabla_{\boldsymbol{\alpha}_{k}} \mathbb{E}_{q_{k+1}} \left[-\log Z(\boldsymbol{\alpha}_{k}) + f_{\boldsymbol{\alpha}_{k}}(\mathbf{z}) \right]$$

$$= \mathbb{E}_{q_{k+1}} \left[\nabla_{\boldsymbol{\alpha}_{k}} f_{\boldsymbol{\alpha}_{k}}(\mathbf{z}) \right] - \mathbb{E}_{p_{\boldsymbol{\alpha}_{k}}} \left[\nabla_{\boldsymbol{\alpha}_{k}} f_{\boldsymbol{\alpha}_{k}}(\mathbf{z}) \right],$$
(A4)

where $p_{\alpha_k} = Z(\alpha_k)^{-1} \exp(f_{\alpha_k}) q_k$; $Z(\alpha_k) = \int_{\mathbf{z}} \exp(f_{\alpha_k}) q_k(\mathbf{z}) d\mathbf{z}$ is the normalizing constant.

B.2 Proof of Proposition 3.1

Proof. Recall that the objective in NTRE for estimating each r_{α_k} is:

$$\lim_{M \to \infty} \mathcal{L}_M(\boldsymbol{\alpha}_k) = \mathbb{E}_{q_{k+1}(\mathbf{z})} \left[\log \frac{r_{\boldsymbol{\alpha}_k}}{M + r_{\boldsymbol{\alpha}_k}} \right] + M \mathbb{E}_{q_k(\mathbf{z})} \left[\log \frac{M}{M + r_{\boldsymbol{\alpha}_k}} \right]. \tag{A5}$$

We can derive the gradient of $\mathcal{L}_M(\alpha_k)$:

$$\nabla_{\boldsymbol{\alpha}_{k}} \mathcal{L}_{M}(\boldsymbol{\alpha}_{k}) = \mathbb{E}_{q_{k+1}(\mathbf{z})} \left[\nabla_{\boldsymbol{\alpha}_{k}} \log \frac{r_{\boldsymbol{\alpha}_{k}}}{M + r_{\boldsymbol{\alpha}_{k}}} \right] + M \mathbb{E}_{q_{k}(\mathbf{z})} \left[\nabla_{\boldsymbol{\alpha}_{k}} \log \frac{M}{M + r_{\boldsymbol{\alpha}_{k}}} \right]. \tag{A6}$$

For the first component, we have

$$\nabla_{\boldsymbol{\alpha}_{k}} \log \frac{r_{\boldsymbol{\alpha}_{k}}}{M + r_{\boldsymbol{\alpha}_{k}}} = -\nabla_{\boldsymbol{\alpha}_{k}} \log \left(1 + \frac{M}{r_{\boldsymbol{\alpha}_{k}}}\right) = \frac{r_{\boldsymbol{\alpha}}}{M + r_{\boldsymbol{\alpha}_{k}}} \frac{M}{r_{\boldsymbol{\alpha}_{k}}} \left(\frac{1}{p_{\boldsymbol{\alpha}_{k}}} \nabla_{\boldsymbol{\alpha}_{k}} p_{\boldsymbol{\alpha}_{k}}\right) = \frac{M}{M + r_{\boldsymbol{\alpha}_{k}}} \nabla_{\boldsymbol{\alpha}_{k}} \log p_{\boldsymbol{\alpha}_{k}}.$$
(A7)

Similarly, for the second component, we have

$$\nabla_{\boldsymbol{\alpha}_{k}} \log \frac{M}{M + r_{\boldsymbol{\alpha}_{k}}} = -\nabla_{\boldsymbol{\alpha}_{k}} \log \left(1 + \frac{r_{\boldsymbol{\alpha}_{k}}}{M} \right) = -\frac{1}{M + r_{\boldsymbol{\alpha}_{k}}} \nabla_{\boldsymbol{\alpha}_{k}} r_{\boldsymbol{\alpha}_{k}}$$

$$= -\frac{r_{\boldsymbol{\alpha}_{k}}}{M + r_{\boldsymbol{\alpha}_{k}}} \left(\frac{1}{p_{\boldsymbol{\alpha}_{k}}} \nabla_{\boldsymbol{\alpha}_{k}} p_{\boldsymbol{\alpha}_{k}} \right) = -\frac{r_{\boldsymbol{\alpha}_{k}}}{M + r_{\boldsymbol{\alpha}_{k}}} \nabla_{\boldsymbol{\alpha}_{k}} \log p_{\boldsymbol{\alpha}_{k}}.$$
(A8)

Plugging Eqs. (A7) and (A8) into Eq. (A6), we have

$$\nabla_{\boldsymbol{\alpha}_{k}} \mathcal{L}_{M}(\boldsymbol{\alpha}_{k}) = \mathbb{E}_{q_{k+1}(\mathbf{z})} \left[\frac{M}{M + r_{\boldsymbol{\alpha}_{k}}} \nabla_{\boldsymbol{\alpha}_{k}} \log p_{\boldsymbol{\alpha}_{k}} \right] - M \mathbb{E}_{q_{k}(\mathbf{z})} \left[\frac{r_{\boldsymbol{\alpha}_{k}}}{M + r_{\boldsymbol{\alpha}_{k}}} \nabla_{\boldsymbol{\alpha}_{k}} \log p_{\boldsymbol{\alpha}_{k}} \right]$$

$$= \mathbb{E}_{q_{k+1}(\mathbf{z})} \left[\frac{M}{M + r_{\boldsymbol{\alpha}_{k}}} \nabla_{\boldsymbol{\alpha}_{k}} \log p_{\boldsymbol{\alpha}_{k}} \right] - \mathbb{E}_{p_{\boldsymbol{\alpha}_{k}}(\mathbf{z})} \left[\frac{M}{M + r_{\boldsymbol{\alpha}_{k}}} \nabla_{\boldsymbol{\alpha}_{k}} \log p_{\boldsymbol{\alpha}_{k}} \right]$$

$$= \int_{\mathbf{z}} \frac{M}{M + r_{\boldsymbol{\alpha}_{k}}(\mathbf{z})} \left(q_{k+1}(\mathbf{z}) - p_{\boldsymbol{\alpha}_{k}}(\mathbf{z}) \right) \nabla_{\boldsymbol{\alpha}_{k}} f_{\boldsymbol{\alpha}_{k}}(\mathbf{z}) d\mathbf{z}.$$
(A9)

Therefore, we can see that

$$\lim_{M \to \infty} \nabla_{\alpha_k} \mathcal{L}_M(\alpha_k) \to \mathbb{E}_{q_{k+1}} [\nabla_{\alpha_k} f_{\alpha_k}(\mathbf{z})] - \mathbb{E}_{p_{\alpha_k}} [\nabla_{\alpha_k} f_{\alpha_k}(\mathbf{z})]. \tag{A10}$$

B.3 Proof of Theorem 3.4

To prove Theorem 3.4, we first prove the following lemma:

Lemma B.1. Assume $p_{\beta}(\mathbf{x}, y | \mathbf{z})$ follows a joint normal distribution with

$$\mathbf{E}(\mathbf{x}^T, y)^T = (\mu_{\mathbf{x}}^T, y)^T, \mathbf{Var}(\mathbf{x}^T, y)^T = \begin{pmatrix} \Sigma_{xx} & \Sigma_{xy} \\ \Sigma_{xy}^T & \Sigma_{yy} \end{pmatrix}, \tag{A11}$$

$$\mathbf{E}(\mathbf{x}|y,z) = \mu_{\mathbf{x}|y}, \mathbf{Var}(\mathbf{x}|y,z) = \Sigma_{xx|y}$$
(A12)

Define

$$\mathbf{U}_{uncon} = \{\mathbf{x} | (\mathbf{x} - \mu_{\mathbf{x}})^T \mathbf{\Sigma}_{xx}^{-1} (\mathbf{x} - \mu_{\mathbf{x}}) \le R\}, \mathbf{U}_{con} = \{\mathbf{x} | (\mathbf{x} - \mu_{\mathbf{x}|y})^T \mathbf{\Sigma}_{xx|y}^{-1} (\mathbf{x} - \mu_{\mathbf{x}|y}) \le R\}.$$
(A13)

Then we have

$$\mathbf{U}_{con} - \mu_{\mathbf{x}|y} \subset \mathbf{U}_{uncon} - \mu_{\mathbf{x}} \tag{A14}$$

Proof. Based on the properties of the conditional normal distribution, we can state that

$$\mu_{\mathbf{x}|y} = \mu_{\mathbf{x}} + \Sigma_{xy} \Sigma_{yy}^{-1} (\mathbf{y} - \mu_y), \Sigma_{\mathbf{x}|y} = \Sigma_{xx} - \Sigma_{xy} \Sigma_{yy}^{-1} \Sigma_{xy}^T. \tag{A15}$$

According to the Sherman-Morrison-Woodbury formula, we can see that

$$\Sigma_{xx}^{-1} = \Sigma_{\mathbf{x}|y}^{-1} - \frac{\Sigma_{\mathbf{x}|y}^{-1} \Sigma_{xy} \Sigma_{yy}^{-1} \Sigma_{xy}^{T} \Sigma_{\mathbf{x}|y}^{-1}}{1 + \Sigma_{yy}^{-1} \Sigma_{xy}^{T} \Sigma_{xy}^{-1} \Sigma_{xy}^{-1}}.$$
(A16)

Note that since $\Sigma_{\mathbf{x}|y}$ is a positive definite matrix, $\Sigma_{\mathbf{x}|y}^{-1}$ is also a positive definite matrix, which implies

$$1 + \sum_{yy}^{-1} \sum_{xy}^{T} \sum_{x|y}^{-1} \sum_{xy} > 1 > 0.$$
 (A17)

Besides, $\Sigma_{\mathbf{x}|y}^{-1} \Sigma_{xy} \Sigma_{yy}^{-1} \Sigma_{xy}^T \Sigma_{\mathbf{x}|y}^{-1} = \Sigma_{yy}^{-1} \{\Sigma_{\mathbf{x}|y}^{-1} \Sigma_{xy}\} \{\Sigma_{\mathbf{x}|y}^{-1} \Sigma_{xy}\}^T$ is also a semi-positive definite matrix, therefore $\frac{\Sigma_{\mathbf{x}|y}^{-1} \Sigma_{xy} \Sigma_{yy}^{-1} \Sigma_{xy}^T \Sigma_{\mathbf{x}|y}^{-1}}{1 + \Sigma_{yy}^{-1} \Sigma_{xy}^T \Sigma_{\mathbf{x}|y}^{-1} \Sigma_{xy}}$ is semi-positive definite, which means

$$\mathbf{a}^T \Sigma_{xx}^{-1} \mathbf{a} \le \mathbf{a}^T \Sigma_{\mathbf{x}|y}^{-1} \mathbf{a}, \ \forall \mathbf{a}, \tag{A18}$$

so $\forall \mathbf{x}$ such that

$$(\mathbf{x} - \mu_{\mathbf{x}|y})^T \mathbf{\Sigma}_{\mathbf{x}|y}^{-1} (\mathbf{x} - \mu_{\mathbf{x}|y}) \le R, \tag{A19}$$

we have

$$(\mathbf{x} - \mu_{\mathbf{x}|y})^T \mathbf{\Sigma}_{xx}^{-1} (\mathbf{x} - \mu_{\mathbf{x}|y}) \le R, \tag{A20}$$

namely

$$(\mathbf{x} - \mu_{\mathbf{x}|y} + \mu_{\mathbf{x}} - \mu_{\mathbf{x}})^T \Sigma_{xx}^{-1} (\mathbf{x} - \mu_{\mathbf{x}|y} + \mu_{\mathbf{x}} - \mu_{\mathbf{x}}) \le R.$$
(A21)

Therefore we have

$$\mathbf{U}_{con} - \mu_{\mathbf{x}|y} + \mu_{\mathbf{x}} \subset \mathbf{U}_{uncon}, \tag{A22}$$

namely

$$\mathbf{U}_{con} - \mu_{\mathbf{x}|y} \subset \mathbf{U}_{uncon} - \mu_{\mathbf{x}},\tag{A23}$$

which finishes the proof.

Now we are ready to prove Theorem 3.4.

 $\begin{aligned} & \textit{Proof.} \ \, \forall \alpha \in (0,1), \ \, \text{define} \ \, \mathbf{U}_{uncon}(\alpha) = \{\mathbf{x} | (\mathbf{x} - \mu_{\mathbf{x}})^T \mathbf{\Sigma}_{xx}^{-1} (\mathbf{x} - \mu_{\mathbf{x}}) \leq \chi_p^2(\alpha) \} \ \, \text{and} \ \, \mathbf{U}_{con}(\alpha) = \{\mathbf{x} | (\mathbf{x} - \mu_{\mathbf{x}|y})^T \mathbf{\Sigma}_{xx|y}^{-1} (\mathbf{x} - \mu_{\mathbf{x}|y}) \leq \chi_p^2(\alpha) \}, \ \, \text{where} \ \, \chi_p^2(\alpha) \ \, \text{is the} \ \, \alpha \ \, \text{quantile of} \ \, \chi_p^2, \ \, \text{then we have} \\ & \mathbf{P}_{\mathbf{x}|z}(\mathbf{U}_{uncon}(\alpha)) = \mathbf{P}_{\mathbf{x}|y,z}(\mathbf{U}_{con}(\alpha)) = \alpha, \ \, \text{and also according to Lemma B.1,} \end{aligned}$

$$\mathbf{U}_{con}(\alpha) - \mu_{\mathbf{x}|y} \subset \mathbf{U}_{uncon}(\alpha) - \mu_{\mathbf{x}}, \tag{A24}$$

namely

$$\mathbf{U}_{con}(\alpha) - \mu_{\mathbf{x}|y} + \mu_{\mathbf{x}} \subset \mathbf{U}_{uncon}(\alpha), \tag{A25}$$

which finishes the proof.

B.4 Proof of Proposition 3.6

Proof. Equivalently, we can write $\mathcal{L}_M(\alpha_k)$ as

$$\mathcal{L}_{M}(\boldsymbol{\alpha}_{k}) = \mathbb{E}_{q_{k+1}(\mathbf{z})} \left[\log \sigma \left(\tilde{f}_{\boldsymbol{\alpha}_{k}} - \log M \right) \right] + M \mathbb{E}_{q_{k}(\mathbf{z})} \left[\log \left(1 - \sigma \left(\tilde{f}_{\boldsymbol{\alpha}_{k}} - \log M \right) \right) \right]$$

$$= \mathbb{E}_{q_{k+1}} \log s + M \mathbb{E}_{q_{k}} \log(1 - s) = \mathcal{J}(s).$$
(A26)

where $\sigma(\cdot)$ is the sigmoid function, $\tilde{f}_{\alpha_k} = \log r_{\alpha_k}$, and that $s = \sigma\left(\tilde{f}_{\alpha_k} - \log M\right)$.

For $\epsilon > 0$ and a perturbation $u(\mathbf{z})$ (testing function), we can see that

$$\begin{split} \mathcal{J}(s+\epsilon u) - cJ(s) &= \mathbb{E}_{q_{k+1}} \log(s+\epsilon u) + M\mathbb{E}_{q_k} \log(1-s-\epsilon u) \mathbb{E}_{q_{k+1}} \log s - M\mathbb{E}_{q_k} \log(1-s) - \\ &= \mathbb{E}_{q_{k+1}} \log\left(1+\epsilon \frac{u}{s}\right) + M\mathbb{E}_{q_k} \log\left(1+\epsilon \frac{-u}{1-s}\right) \\ &= \epsilon \left(\mathbb{E}_{q_{k+1}} \left(\frac{u}{s}\right) + M\mathbb{E}_{q_k} \left(\frac{-u}{1-s}\right)\right) + o(\epsilon). \end{split} \tag{A27}$$

Therefore, we can see that $d\mathcal{J}(s) = 0$ leads to

$$\lim_{\epsilon \to 0} \frac{\mathcal{J}(s+\epsilon u) - cJ(s)}{\epsilon} = \int_{\mathbf{z}} u(\mathbf{z}) \frac{q_{k+1}(\mathbf{z})}{s(\mathbf{z})} d\mathbf{z} - \int_{\mathbf{z}} u(\mathbf{z}) \frac{Mq_k(\mathbf{z})}{1 - s(\mathbf{z})} d\mathbf{z} = 0. \tag{A28} \label{eq:A28}$$

A necessary condition for optimality then emerges as

$$\frac{q_{k+1}(\mathbf{z})}{s(\mathbf{z})} = \frac{Mq_k(\mathbf{z})}{1 - s(\mathbf{z})} \iff s = \frac{q_{k+1}}{Mq_k + q_{k+1}}.$$
(A29)

We can therefore see that the optimal ratio is $r_{\alpha_k}^* = \frac{q_{k+1}}{q_k}$, regardless of the value of M.

B.5 Proof of Theorem 3.8

As in [68], we focus on the exponential family p_{α_k} , where the density can be written as $p_{\alpha_k} = \exp\left(\alpha_k'\tilde{T}(\mathbf{z}) - \log Z(\alpha_k)\right)$. $\tilde{T}(\mathbf{z})$ is the sufficient statistics and $Z(\alpha_k)$ is the partition function.

This can be seen as restricting the \tilde{f}_{α_k} network learnability to the last layer to simplify the analysis. The results can be extended to fully trainable networks by a layer-wise training scheme [97].

Lemma B.2. (Convexity) For $r_{\alpha_k} = \frac{p_{\alpha_k}}{q_k}$, where p_{α_k} represents exponential family of distributions, the negative objective in Eq. (9) is convex in parameter α_k .

Proof. To simplify the notation, we treat the log partition function as an extra parameter. Let τ denote the extended parameter, i.e., $\tau := [\alpha_k, \alpha_{Z_k}]$, where $\alpha_{Z_k} = \log Z(\alpha_k)$ denotes the log partition function. We accordingly extend the sufficient statistics as $T(\mathbf{z}) = [\tilde{T}(\mathbf{z}), -1]$ to account for the log partition function. The density with the extended representation is now $p_{\tau}(\mathbf{z}) = \exp(\tau' T(\mathbf{z}))$. We will use the notation p_{α_k} and p_{τ} interchangeably henceforth. Let τ^* denote the optimal parameter, i.e., $p_{\tau^*} = p^* = q_{k+1}$.

We can first see that $\nabla_{\tau} p_{\tau}(\mathbf{z}) = p_{\tau}(\mathbf{z}) T(\mathbf{z})$. The gradient and Hessian for $\mathcal{L}_{M}(\tau)$ are:

$$\nabla_{\boldsymbol{\tau}} \mathcal{L}_{M}(\boldsymbol{\tau}) = \mathbb{E}_{q_{k+1}} \left[\nabla_{\boldsymbol{\tau}} \log \frac{p_{\boldsymbol{\tau}}}{Mq_{k} + p_{\boldsymbol{\tau}}} \right] + M \mathbb{E}_{q_{k}} \left[\nabla_{\boldsymbol{\tau}} \log \frac{Mq_{k}}{Mq_{k} + p_{\boldsymbol{\tau}}} \right]$$

$$= \mathbb{E}_{q_{k+1}} \left[\frac{(p_{\boldsymbol{\tau}} + Mq_{k}) Mq_{k}}{(p_{\boldsymbol{\tau}} + Mq_{k})^{2}} T \right] - M \mathbb{E}_{q_{k}} \left[\frac{(p_{\boldsymbol{\tau}} + Mq_{k})}{(p_{\boldsymbol{\tau}} + Mq_{k})^{2}} p_{\boldsymbol{\tau}} T \right]$$

$$= \int_{\mathbf{z}} \frac{1}{p_{\boldsymbol{\tau}} + Mq_{k}} \left(Mq_{k+1}q_{k}T - Mp_{\boldsymbol{\tau}}q_{k}T \right) d\mathbf{z}$$

$$= \int_{\mathbf{z}} \frac{Mq_{k}T}{p_{\boldsymbol{\tau}} + Mq_{k}} \left(q_{k+1} - p_{\boldsymbol{\tau}} \right) d\mathbf{z}.$$

$$\nabla_{\boldsymbol{\tau}}^{2} \mathcal{L}_{M}(\boldsymbol{\tau}) = - \int_{\mathbf{z}} \left[\frac{q_{k}T}{(p_{\boldsymbol{\tau}} + Mq_{k})^{2}} \left(Mq_{k+1} - Mp_{\boldsymbol{\tau}} \right) p_{\boldsymbol{\tau}} T + \frac{q_{k}T}{p_{\boldsymbol{\tau}} + Mq_{k}} Mp_{\boldsymbol{\tau}} T \right] d\mathbf{z}$$

$$= - \int_{\mathbf{z}} \left[\frac{p_{\boldsymbol{\tau}}q_{k}T^{2}}{(p_{\boldsymbol{\tau}} + Mq_{k})^{2}} \left(Mq_{k+1} - Mp_{\boldsymbol{\tau}} + Mp_{\boldsymbol{\tau}} + M^{2}q_{k} \right) \right] d\mathbf{z}$$

$$= - \int_{\mathbf{z}} \frac{p_{\boldsymbol{\tau}}q_{k}T^{2}}{(p_{\boldsymbol{\tau}} + Mq_{k})^{2}} M \left(q_{k+1} + Mq_{k} \right) d\mathbf{z}.$$

$$= - \int_{\mathbf{z}} \frac{p_{\boldsymbol{\tau}}q_{k}T^{2}}{(p_{\boldsymbol{\tau}} + Mq_{k})^{2}} M \left(q_{k+1} + Mq_{k} \right) d\mathbf{z}.$$

Hence the negative Hessian is PSD at any τ .

Lemma B.3. (Polynomial condition number for Eq. (9)) Assuming the singular values of the population Fisher matrix are bounded by λ_{\min} and λ_{\max} , the condition number of the Eq. (9) Hessian at the optimum is bounded, i.e., $\kappa^* \lesssim \frac{\lambda_{\max}}{\lambda_{\min}}$.

Proof. We would like to bound the ratio $\frac{\mathbf{v}'\nabla_{\tau}^{2}\mathcal{L}_{M}(\tilde{\tau})\mathbf{v}}{\mathbf{v}'\nabla_{\tau}^{2}\mathcal{L}_{M}(\tau^{*})\mathbf{v}}$ for any unit vector \mathbf{v} . Denote $\tilde{p} = \exp\left(\tilde{\tau}'T\right) = \exp\left(\left(\tau^{*} + \boldsymbol{\delta}\right)'T\right) = p^{*}\exp\left(\boldsymbol{\delta}'T\right)$. We can see that

$$\lim_{M \to \infty} \mathbf{v}' \nabla_{\boldsymbol{\tau}}^{2} \mathcal{L}_{M}(\tilde{\boldsymbol{\tau}}) \mathbf{v} = -\lim_{M \to \infty} \int_{\mathbf{z}} \frac{p^{*} \exp\left(\boldsymbol{\delta}'T\right) q_{k}}{\left(p^{*} \exp\left(\boldsymbol{\delta}'T\right) + M q_{k}\right)^{2}} M\left(q_{k+1} + M q_{k}\right) \left(\mathbf{v}'T\right)^{2} d\mathbf{z}$$

$$= -\int_{\mathbf{z}} p^{*} \exp\left(\boldsymbol{\delta}'T\right) \left(\mathbf{v}'T\right)^{2} d\mathbf{z} = -\mathbb{E}_{\tilde{\boldsymbol{\tau}}} \left(\mathbf{v}'T\right)^{2}$$

$$\lim_{M \to \infty} \mathbf{v}' \nabla_{\boldsymbol{\tau}}^{2} \mathcal{L}_{M}(\boldsymbol{\tau}^{*}) \mathbf{v} = -\lim_{M \to \infty} \int_{\mathbf{z}} \frac{p^{*} q_{k}}{\left(p^{*} + M q_{k}\right)^{2}} M\left(q_{k+1} + M q_{k}\right) \left(\mathbf{v}'T\right)^{2} d\mathbf{z}$$

$$= -\lim_{M \to \infty} \int_{\mathbf{z}} \frac{M p^{*} q_{k}}{p^{*} + M q_{k}} \left(\mathbf{v}'T\right)^{2} d\mathbf{z}$$

$$= -\int_{\mathbf{z}} p^{*} \left(\mathbf{v}'T\right)^{2} d\mathbf{z} = -\mathbb{E}_{\boldsymbol{\tau}^{*}} \left(\mathbf{v}'T\right)^{2}.$$
(A31)

Therefore, we can see that under Assumption B.5,

$$\frac{\lambda_{\min}}{\lambda_{\max}} \leq \lim_{M \to \infty} \frac{\mathbf{v}' \nabla_{\boldsymbol{\tau}}^{2} \mathcal{L}_{M}(\tilde{\boldsymbol{\tau}}) \mathbf{v}}{\mathbf{v}' \nabla_{\boldsymbol{\tau}}^{2} \mathcal{L}_{M}(\boldsymbol{\tau}^{*}) \mathbf{v}} = \frac{\mathbb{E}_{\tilde{\boldsymbol{\tau}}} \left(\mathbf{v}' T \right)^{2}}{\mathbb{E}_{\boldsymbol{\tau}^{*}} \left(\mathbf{v}' T \right)^{2}} \leq \frac{\lambda_{\max}}{\lambda_{\min}}.$$
(A32)

Hence the NTRE loss satisfies Assumption B.6 with constants $\beta_u = \frac{\lambda_{\max}}{\lambda_{\min}}$ and $\beta_l = \frac{\lambda_{\min}}{\lambda_{\max}}$.

Remark B.4. Lemmas B.2 and B.3 together indicate that the NTRE objective is well-conditioned for optimization. Specifically, it leads to the following result: normalized gradient-based method can find a parameter estimate using Eq. (9) efficiently for α_k , where the number of steps required is polynomial in the distance between the initial estimate and the optimum.

Assumption B.5. (Bounded singular values of the population Fisher matrix) There exist λ_{\max} , $\lambda_{\min} > 0$, such that $\forall \tau \in \mathcal{T}$, we have $\sigma_{\max}(\mathbb{E}_{\tau}[T(\mathbf{z})T(\mathbf{z})']) \leq \lambda_{\max}$, and $\sigma_{\min}(\mathbb{E}_{\tau}[T(\mathbf{z})T(\mathbf{z})']) \geq \lambda_{\min}$.

Assumption B.6. (Bounded Hessian) Under Assumption B.5, it holds that $\sigma_{\max}(\mathbf{H}(\tau)) \leq \beta_u \cdot \sigma_{\max}(\mathbf{H}(\tau^*))$, and $\sigma_{\min}(\mathbf{H}(\tau)) \geq \beta_l \cdot \sigma_{\min}(\mathbf{H}(\tau^*))$, for some constants $\beta_u, \beta_l > 0$.

Assumption B.7. (Bounded parameter norm) $\|\boldsymbol{\alpha}_k\|_2 \leq \omega, \ \forall \boldsymbol{\alpha}_k \in \mathcal{A}.$

Assumption B.8. (Lipschitz log partition function) Assume the log partition function is β_Z -Lipschitz, that is, $\forall \alpha_{k1}, \alpha_{k2} \in \mathcal{A}, |\log Z(\alpha_{k1}) - \log Z(\alpha_{k1})| \leq \beta_Z ||\alpha_{k1} - \alpha_{k2}||_2$.

Theorem B.9. (Theorem 5.1 from Liu et al. [68], restated) Let \mathcal{L} be any loss function that is convex (concave) in the exponential family parameter and satisfies Assumption B.5, Assumption B.6, Assumption B.7, and Assumption B.8. Furthermore, let p^*, q be exponential family distributions with parameters τ^*, τ_q and let κ^* be the condition number of the Hessian at $p = p^*$. Then, for any $0 < \delta \le \frac{1}{\beta_Z}$ and parameter initialization τ_0 , with step size $\eta \le \sqrt{\frac{\beta_l}{\beta_u \kappa^*}} \delta$, performing normalized gradient descent on the population objective \mathcal{L} guarantees that after $T \le \frac{\beta_u \kappa^*}{\beta_l} \frac{\|\tau_0 - \tau^*\|_2^2}{\delta^*}$ steps, there exists an iterate $t \le T$ such that $\|\tau_0 - \tau^*\|_2 \le \delta$.

Proof. Theorem 3.8 follows directly from Theorem B.9, using the condition number bound and constants from Lemma B.3.

C Interpretation of Optimization as Gradient-Based Sampling

In order to extrapolate as far as possible, while still staying on the actual manifold of high-value observations, we need to measure the validity of the generated samples ${\bf x}$ as in [15]. We identify that the value of y from $p_{\beta,y}(y|{\bf z})$ serves as one good indicator as in [10]. The generated samples ${\bf x}$, associated with function values similar to existing y values in the offline dataset, are likely indistribution; those where the $p_{\beta,y}(y|{\bf z})$ predicts a very different score (often erroneously large, see Fig. 2 when y>1) can be too far outside the training distribution [10, 11, 19]. In addition, ideally, after training we have a well-learned and informative latent space prior model p_{α} that i) captures the multiple possible modes of the one-to-many inverse mapping, and ii) faithfully assigns the function values to observations through the joint latent space (Fig. 2 and 4). Taking together, we can optimize over ${\bf z}$ in the latent space to find the best, most trustworthy ${\bf x}$ subject to the following constraints: i) ${\bf z}$ has a high likelihood under p_{α} and ii) the predicted function value associated with ${\bf z}$ is not too different from the value $y_{\rm max}$. This can be formulated as the following optimization problem:

$$\arg\max_{y(\mathbf{z})} y = g_{\beta}(\mathbf{z}) \ s.t. \ p_{\beta}(y_{\text{max}}|\mathbf{z}) > \epsilon_1, \ p_{\alpha}(\mathbf{z}) > \epsilon_2.$$
(A33)

The above constrained optimization problem is conceptually similar to the formulation mentioned in [10] Sec. 3.2. The $p_{\beta}(y_{\text{max}}|\mathbf{z}) > \epsilon_1$ constraint enforces that \mathbf{z} stays on the manifold of high-value observations as we discussed; the $p_{\alpha}(\mathbf{z}) > \epsilon_2$ constraint encourages extrapolating beyond the best score in the offline dataset \mathcal{D} by providing meaningful gradient during the optimization (see Sec. 4.3 for more empirical evidence).

In our set-up, the unnormalized log-density of $p_{\gamma}(\mathbf{z}|y) \propto p_{\beta,y}(y|\mathbf{z})p_{\alpha}(\mathbf{z})$ given the best offline function value y_{\max} can be written as $-\lambda_1\|y_{\max}-g_{\beta,y}(\mathbf{z})\|_2^2+\lambda_2\left(\sum_{k=0}^K \tilde{f}_{\alpha_k}(\mathbf{z})-\frac{1}{2}\|\mathbf{z}\|_2^2\right)$, where λ_1 is the variance of $p_{\beta,y}(y|\mathbf{z})=\mathcal{N}(g_{\beta,y}(\mathbf{z}),\sigma_y^2\mathbf{I})$ and λ_2 re-weights the prior term. This is equivalent to optimizing the Lagrangian of Eq. (A33), with the density constraints modified to be log-densities. In practice, we employ SVGD to fully utilize the informative latent space during optimization. Ideally, the dual variables, λ_1 and λ_2 are supposed to be optimized together with y and z, however, we find it convenient to choose them to be fixed as a constant throughout, at $\lambda_1=20.0$ and $\lambda_2=1.0$, analogous to penalty methods in constrained optimization. The same values of λ_1 and λ_2 are used for all domains in our experiments.

D Network Architecture and Implementation Details

Architecture We provide detailed network architecture for the log-ratio estimator $\tilde{f}_{\alpha_k}(\mathbf{z},k)$ in Tab. A1; we adopt the same architecture throughout the experiments. The generator networks for \mathbf{x} and y is a 5-layer MLP structure shown in Tab. A2. We employ a single network that directly outputs the (\mathbf{x},y) pair to implement $g_{\boldsymbol{\beta},\mathbf{x}}, g_{\boldsymbol{\beta},y}$. For discrete tasks, the $g_{\boldsymbol{\beta},\mathbf{x}}$ head outputs logits for reconstruction. The encoder network to embed the input is a 3-layer MLP, as shown in Tab. A2. For discrete tasks, we add an additional embedding layer to map discrete inputs to continuous vectors. The architectures are shared across different task domains; we only adjust the input size for different tasks. For function values y and continuous \mathbf{x} , we normalize these values for training using the offline dataset maxium $\mathbf{x}_{\max}, y_{\max}$ and minimum $\mathbf{x}_{\min}, y_{\min}$: $\mathbf{x}_{\text{train}} = \frac{\mathbf{x} - \mathbf{x}_{\min}}{\mathbf{x}_{\max} - \mathbf{x}_{\min}}$. $y_{\text{train}} = \frac{y - y_{\min}}{y_{\max} - y_{\min}}$.

Table A1: Network architecture for the log-ratio estimator $\tilde{f}_{\alpha_k}(\mathbf{z},k)$. N is set to 16 for all the experiments. $d_{\mathbf{z}}=20$ is the latent space dimension used for all experiments.

Table A2: Generator and encoder network architectures. LReLU indicates the Leaky-ReLU activa-
tion function. $d_{\mathbf{x}}$ is the dimension of input \mathbf{x} men-
tioned in Tab. A3. For discrete tasks, $d_{\mathbf{x}}$ specifies the
length of input, and L denotes number of possible
discrete tokens.

Layers	Output size	Note		Comment	
	I. J. F.			Generator	
	Indx. Emb.		Layers	Out Size	Note
Input: k	1	stage indx. of NTRE	Input: z	$d_{\mathbf{z}} = 20$	
G: 1	100	OINIKE	Linear, LReLU	128	
Sin. emb.	128		Linear, LReLU	64	neg_slope
Linear, LReLU	128	neg_slope	Linear, LReLU	32	0.2^{-1}
Linear	128	0.2	Linear, LReLU	32	••• <u>•</u>
Linear			C	ontinuous Outp	ut
	Input Emb.		Linear	$d_{\mathbf{x}} + 1$	output (\mathbf{x}, y)
Input: z	$d_{\mathbf{z}} = 20$			Discrete Output	
Linear, LReLU	128	neg_slope 0.2	Linear	$d_{\mathbf{x}} \times L + 1$	num. tokens. ${\cal L}$
Linear	128	0.2		Encoder	
Linear			Layers	Encoder Out Size	Note
Linear Input: z , t	$ \frac{128}{\tilde{\mathbf{f}}_{\alpha_{\mathbf{k}}}(\mathbf{z}, \mathbf{k})} $ $ 1, d_{\mathbf{z}} = 20 $		Layers		Note
Input: z , t	$\mathbf{\tilde{f}_{\alpha_k}(z, k)}$ $1, d_z = 20$	Emb. of		Out Size Embedding	
	$\mathbf{ ilde{f}_{lpha_{k}}(z,k)}$			Out Size	
Input: \mathbf{z}, t Input & Indx.	$\mathbf{\tilde{f}_{\alpha_k}(z, k)}$ $1, d_z = 20$	Emb. of	(f	Out Size Embedding or discrete x onl	y)
Input: z , <i>t</i> Input & Indx. Emb. Concat.	$ \begin{aligned} \tilde{\mathbf{f}}_{\alpha_{\mathbf{k}}}(\mathbf{z}, \mathbf{k}) \\ 1, d_{\mathbf{z}} &= 20 \\ 128 \times 2 \\ 256 \end{aligned} $	Emb. of	Input: x	Out Size Embedding for discrete \mathbf{x} onl $32 \times d_{\mathbf{x}}$	y) emb. \mathbf{x} input (\mathbf{x}, y)
Input: z , <i>t</i> Input & Indx. Emb.	$\mathbf{\tilde{f}_{\alpha_k}(z, k)}$ $1, d_z = 20$ 128×2	Emb. of each input	Input: \mathbf{x} concat (\mathbf{x}, y)	Out Size Embedding or discrete \mathbf{x} onl $32 \times d_{\mathbf{x}}$ $(32 \times) d_{\mathbf{x}} + 1$	y) emb. x
Input: z , <i>t</i> Input & Indx. Emb. Concat. LReLU, Linear	$ \begin{aligned} \tilde{\mathbf{f}}_{\alpha_{\mathbf{k}}}(\mathbf{z}, \mathbf{k}) \\ 1, d_{\mathbf{z}} &= 20 \\ 128 \times 2 \\ 256 \\ 128 \end{aligned} $	Emb. of each input	Input: \mathbf{x} concat (\mathbf{x}, y) Linear, LReLU	Out Size Embedding or discrete \mathbf{x} onl $32 \times d_{\mathbf{x}}$ $(32 \times) d_{\mathbf{x}} + 1$ 128	y) emb. \mathbf{x} input (\mathbf{x}, y) neg_slope
Input: z , <i>t</i> Input & Indx. Emb. Concat.	$ \begin{aligned} \tilde{\mathbf{f}}_{\alpha_{\mathbf{k}}}(\mathbf{z}, \mathbf{k}) \\ 1, d_{\mathbf{z}} &= 20 \\ 128 \times 2 \\ 256 \end{aligned} $	Emb. of each input neg_slope 0.2	Input: \mathbf{x} concat (\mathbf{x}, y) Linear, LReLU	Out Size Embedding or discrete \mathbf{x} onl $32 \times d_{\mathbf{x}}$ $(32 \times) d_{\mathbf{x}} + 1$ 128 128	y) emb. \mathbf{x} input (\mathbf{x}, y) neg_slope
Input: z , <i>t</i> Input & Indx. Emb. Concat. LReLU, Linear	$ \begin{aligned} \tilde{\mathbf{f}}_{\alpha_{\mathbf{k}}}(\mathbf{z}, \mathbf{k}) \\ 1, d_{\mathbf{z}} &= 20 \\ 128 \times 2 \\ 256 \\ 128 \end{aligned} $	Emb. of each input neg_slope 0.2 LReLU, Linear	Input: \mathbf{x} concat (\mathbf{x}, y) Linear, LReLU Linear, LReLU	Out Size Embedding or discrete \mathbf{x} onl $32 \times d_{\mathbf{x}}$ $(32 \times) d_{\mathbf{x}} + 1$ 128 128 Mean head	y) emb. \mathbf{x} input (\mathbf{x}, y) neg_slope

Hyperparameters and implementation details As mentioned in Sec. 3.2, we use the linear schedule as in [30, 67] to specify σ_k^2 and construct the intermediate distributions $\{q_k\}_{k=0}^K$. We set the number of stages to 6, *i.e.*, K+1=6. Specifically, the sequence of $\{\sigma_k^2\}_{k=0}^5$ is: $\{\sigma_k^2\}_{k=0}^5 = [0.01, 0.3237, 0.5165, 0.6322, 0.7132, 0.7734, 0.9997]$. To estimate the Eq. (9), we can use monte carlo average: $\mathcal{L}_{M\to\infty}(\alpha_k)\approx\frac{1}{n_1}\sum_{i=1}^{n_1}\left[\log\frac{r_{\alpha_k}(\mathbf{z}_i)}{M+r_{\alpha_k}(\mathbf{z}_i)}\right]+\frac{M}{n_2}\sum_{j=1}^{n_2}\left[\log\frac{M}{M+r_{\alpha_k}(\mathbf{z}_j)}\right]$, where $\mathbf{z}_i\sim q_{k+1},\mathbf{z}_j\sim q_k$. We follow Mnih and Teh [66] and set $n_2=Mn_1$ in practice, where M=100 for all experiments; n_1 is the batch size. When training with Eq. (7), we set the weight for reconstructing \mathbf{x} and predicting y to 50 for the term $\mathbb{E}_{q_{\phi}}[\log p_{\beta}(\mathbf{x},y|\mathbf{z})]$. We set the weight for controlling how fast q_{ϕ} and p_{α} run towards each other to 0.75 for the term $\mathbb{D}_{\mathrm{KL}}(q_{\phi}||r_{\alpha_K}q_K) - \sum_{k=0}^{K-1}\mathbb{D}_{\mathrm{KL}}(q_{k+1}||r_{\alpha_k}q_k)$. Additionally, we apply orthogonal regularization [98] to the parameters of generator networks, with a weight of 0.001 to facilitate training. These hyperparameters are shared across all the experiments.

The parameters of all the networks are initialized with the default pytorch methods [99]. We use the Adam optimizer [100] with $\beta_1 = 0.5$ and $\beta_2 = 0.999$ to train the generator and encoder networks; the log-ratio estimator network is trained with default (β_1, β_2) . The initial learning rates of the generator and encoder networks are 1e-4, and 5e-5 for the log-ratio network. We further perform gradient

clipping by setting the maximal gradient norm as 100 for these networks. We run the experiments on a A6000 GPU with the batch size of 128. Training typically converges within 30K iterations on all the datasets. Running an experiment on one dataset from [21] typically consumes 12-24 hours.

When sampling with SVGD for optimization, the number of SVGD iterations T is set to 500. For all experiments, we use RBF kernel $k(\mathbf{z}, \mathbf{z}_0) = \exp\left(-\frac{1}{2h^2}\|\mathbf{z} - \mathbf{z}_0\|_2^2\right)$ for SVGD, and set the bandwidth to be $h^2 = \frac{\mathrm{med}^2}{2\log(n+1)}$. med is the median of the pairwise distance between the current samples $\{\mathbf{z}_i^t\}_{i=1}^Q$; this follows the same heuristic as in [64] that $\sum_j k(\mathbf{z}_i, \mathbf{z}_j) \approx n \exp\left(-\frac{1}{2h^2}\mathrm{med}^2\right) = 1$. We can balance the contribution from its own gradient and the influence from the other points for each sample \mathbf{z}_i . Of note, the bandwidth changes adaptively across iterations with this heuristic. For stability, we use Adam [100] with default hyperparemters instead of AdaGrad [101] used in [64] to allow for adaptive step size ϵ_t when updating with Eq. (5). The initial step size is set to values with in the range of [0.3, 0.5] for different tasks. We average over 5 and 8 runs to report the means and variances in Tabs. 2 and 3 following [11, 18].

Code We promise to release code, data and model weights upon acceptance of this manuscript.

E Additional Experiment Details & Supplementary Results

E.1 2D Branin Function

Branin is a well-known function for benchmarking optimization methods. We consider the negative of the standard 2D Branin function in the range $x_1 \in [-5, 10], x_2 \in [0, 15]$:

$$f_{br}(x_1, x_2) = -a(x_2 - bx_1^2 + cx_1 - r)^2 - s(1 - t)\cos x_1 - s,$$
(A34)

where a=1, $b=\frac{5.1}{4\pi^2}$, $c=\frac{5}{\pi}$, r=6, s=10, and $t=\frac{1}{8\pi}$. In this square region, f_{br} has three global maximas, $(-\pi, 12.275)$, $(\pi, 2.275)$, and (9.425, 2.475); with the maximum value of -0.398 (Fig. 3). The GA baseline uses the offline dataset to train a forward prediction model parameterized by a 2-layer MLP mapping \mathbf{x} to y and then performs gradient ascent on \mathbf{x} to infer its optima. DDOM and BONET follow their default implementation. For the typical forward method, GA in the data space, the problem of assigning an input \mathbf{x} with erroneously large value is clear even in this 2D toy example; the proposed points often violates the square domain constraints [19].

E.2 Design-Bench

E.2.1 Task Overview

The goal of **TF-Bind-8** and **TF-Bind-10** is to optimize for a DNA sequence that has a maximum affinity to bind with a particular transcription factor. The sequences are of length 8 for **TF-Bind-8** and 10 for **TF-Bind-10**, where each element in the sequence is one of 4 bases. **ChEMBL** optimizes drugs for specific chemical properties. In **D'Kitty** and **Ant Morphology**, one need to optimize for the morphology of robots. In **Superconductor**, the goal is to find a material with a high critical temperature. These tasks contain neither personally identifiable nor offensive information. We present detailed information on the tasks we evaluate on in Design-Bench [21] as below in Tab. **A3**. **SIZE** denotes the training dataset size, and **NUM. TOKS** denotes the number of tokens for discrete tasks.

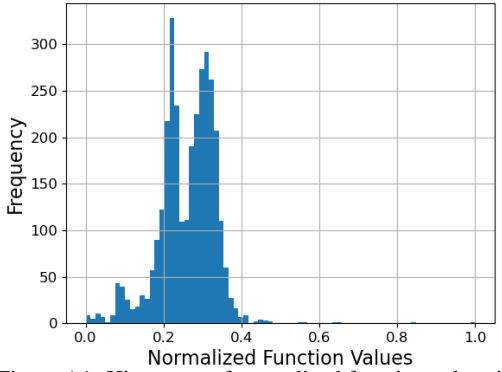
TASK	SIZE	INPUT DIM.	NUM. TOKS	TASK MAX
TF-Bind-8	32898	8	4	1.0
TF-Bind-10	10000	10	4	2.128
ChEMBL	441	31	185	443000.0
D'Kitty	10004	56	-	340.0
Ant	10004	60	-	590.0
Superconductor	17014	86	-	185.0

Table A3: Design-Bench dataset statistics.

E.2.2 HopperController & NAS

As in Krishnamoorthy et al. [11] and Mashkaria et al. [19], we exclude the HopperController task in our results due to significant inconsistencies between the offline dataset values and the values

obtained when running the oracle (see Fig. A1 and A2). This is a known bug in Design-bench (see details in the link). Therefore, we decided not to include Hopper in our evaluation and analysis. Following Krishnamoorthy et al. [11], we exclude NAS due to excessive computation cost required beyond our budget for evaluating across multiple seeds.



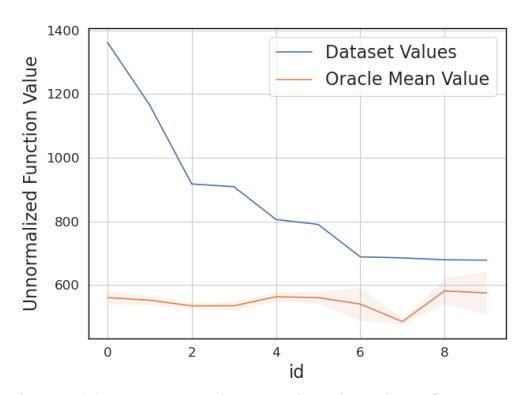


Figure A1: Histogram of normalized function values in the Hopper dataset. The distribution is highly skewed towards low function values (plot from [19]).

Figure A2: Dataset values vs Oracle values for top 10 points. We can see from mean and standard deviation over 20 runs that oracle is noisy (plot from [19]).

E.2.3 Baselines

As mentioned in Sec. 4.2, we compare our method with three groups of baselines: i) sampling via generative inverse models with different parameterizations, including CbAS [1], Auto.CbAS [9], MIN [10] and DDOM to validate our model design; ii) gradient(-like) updating from existing designs, e.g., GA-based [13, 15–18, 22] and BONET and iii) baselines mentioned in [21]. The generative inverse models learn $p_{\theta}(\mathbf{x}|y)$ with different parameterizations and then perform conditional sampling of the high-value designs for BBO. CbAS [1] directly models $p_{\theta}(\mathbf{x}|y)$, while introducing the joint distribution of x and z to facilitate importance sampling. It trains a VAE model to parameterize the distribution using identified high-quality inputs x (by thresholding); it gradually adapts the distribution to the high-value part by refining the threshold. MIN [10] learns $p_{\theta}(\mathbf{x}|y) \propto \mathbb{E}_{p(\mathbf{z}|y)}[p(\mathbf{x}|\mathbf{z},y)]$ with a conditional GAN-like model to instantiate $p(\mathbf{x}|\mathbf{z},y)$ [83, 84]. The method optimizes over \mathbf{z} given the offline dataset maximum y_{max} and map z back to x for BBO solutions. The optimization process over z draw approximate samples from $p(\mathbf{z}|y)$. DDOM [11] consider directly parameterizing the inverse mapping $p_{\theta}(\mathbf{x}|y)$ with a conditional diffusion model in the input design space utilizing the expressiveness of DDPMs [67]. The second group includes the gradient(-like) updating methods, and has the flavor of forward methods in general. The baseline methods include: (i) Gradient Ascent: operates directly on the learned surrogates to propose new input designs via simple gradient ascent; (ii) COMs [15]: regularizes the NN-parameterized surrogate by assigning lower function values to designs obtained during the gradient ascent process; (iii) ROMA [14]: incorporates prior knowledge about function smoothness into the surrogate and optimizes the design against the proxy; (iv) NEMO [13]: leverages normalized maximum likelihood to constrain the distance between the surrogate and the ground-truth; (v) BDI [16]: proposes to distill the information from the static dataset into the high-scoring design; (vi) IOM [17]: enforces the invariance between the representations of the static dataset and generated designs to achieve a natural trade-off; (vii) ICT [18] explores using a pseudo-labeler to generate valuable data for fine-tuning the surrogate. BONET [19] trains a transformer-based model to mimic the optimization trajectories of black-box optimizers, and rolls out evaluation trajectories from the trained model for optimization.

In addition to these recent works, we also compare with several baseline methods described in [21]: 1) GP-qEI [26]: instantiates BO using a Gaussian Process as the uncertainty quantifier and the quasi-Expected Improvement (q-EI) acquisition function, 2) CMA-ES [102]: an evolutionary algorithm that maintains a belief distribution over the optimal candidates; it gradually refines the distribution by adapting the covariance matrix towards optimal candidates using feedback from the learned surrogate, and 3) REINFORCE [73]: first learns a proxy function and then optimizes the input space distribution by leveraging the proxy and the policy-gradient estimator. Since we are in the offline setting, for active methods like BO, we follow the procedure of [21] and optimize on a surrogate model trained on the offline dataset.

For Q=128 results in Tab. 3, we additionally include ExPT [20] and BOOTGEN [12] for rough reference. Of note, these two methods have slightly different set-ups, and are therefore not directly comparable to other baselines and our method. ExPT [20] focuses extensively on few-shot learning scenarios with models pre-trained on larger datasets. BOOTGEN [12] focuses specifically on optimizing biological sequences.

E.2.4 Additional Results & Analysis

Proof-of-concept results for sample complexity First, we uniformly sample N=5000 and N=50 points from the branin function domain for training. We observe that our method i) performs consistently better than BONET [19] and gradient ascent, and ii) demonstrates less performance drop compared with BONET when dataset size is significantly reduced. Further, we use the D'Kitty dataset and withhold an x% size subsection of data, *i.e.*, 0% represents the full dataset. We have similar observation on these datasets summarized in Tabs. A4 and A5, where our method shows much less performance drop compared with the transformer-based method BONET.

Table A4: Results on (reduced size) Branin function dataset.

N	\mathcal{D} (best)	Grad. Ascent	BONET	Ours
5000	-6.199	-3.95 ± 4.26	-1.79 ± 0.84	-0.41 ± 0.13
50	-6.231	-4.64 ± 3.17	-2.13 ± 0.15	-0.43 ± 0.12

Table A5: **Results on (reduced size) D'Kitty dataset.** x% indicates the proportion of training data withheld, *i.e.*, 0% represents the full dataset.

	0%	90%	99%
BONET Ours	$285.11 \pm 15.13 \\ 293.33 \pm 7.45$	$\begin{array}{c} 274.11 \pm 7.57 \\ 289.67 \pm 7.86 \end{array}$	$\begin{matrix} 241.17 \pm 18.07 \\ 283.65 \pm 9.23 \end{matrix}$

Numerical results of $\frac{M}{M+r_{\alpha_k}(\mathbf{z})}$ Recall that we set M=100 for implementing Eq. (9). We examine $v_{100}=\frac{100}{100+r_{\alpha_k}(\mathbf{z})}$ by calculating the average value of it, \bar{v}_{100} , within a batch of $(\mathbf{z}_{k+1},\mathbf{z}_k)\sim (q_{k+1},q_k)$ samples. On all the 6 design-bench datasets used in our experiments, we observe that $\bar{v}_{100}\geq 0.99, k=0,...,5$ from all the trained ratio estimators. It suggests that M=100 is a practical choice for implementing Eq. (9).

Additional results for Q = 256

Unnormalized results For reference, we present the unnormalized results of Tab. 2 in Tab. A6.

Table A6: **Results on design-bench. Unnormalized** results with a budget Q = 256.

BASELINE	TFBIND8	TFBIND10	CHEMBL	SUPERCON.	ANT	D'KITTY
\mathcal{D} (best)	0.439	0.00532	383700.000	74.0	165.326	199.363
GP-qEI CMA-ES REINFORCE	0.824 ± 0.086 0.933 ± 0.035 0.959 ± 0.013	0.675 ± 0.043 0.848 ± 0.136 0.692 ± 0.113	387950.000 ± 0.000 388400.000 ± 400.000 388400.000 ± 2100.000	$\begin{array}{c} 92.686 \pm 3.944 \\ 90.821 \pm 0.661 \\ 89.027 \pm 3.093 \end{array}$	480.049 ± 0.000 $\mathbf{1016.409 \pm 906.407}$ -131.907 ± 41.003	213.816 ± 0.000 4.700 ± 2.230 -301.866 ± 246.284
Gradient Ascent COMs BONET	$\begin{array}{c} 0.981 \pm 0.015 \\ \hline 0.964 \pm 0.020 \\ 0.975 \pm 0.004 \end{array}$	0.770 ± 0.154 0.750 ± 0.078 0.855 ± 0.139	$\begin{array}{c} 390050.000 \pm 2000.000 \\ 390200.000 \pm 500.000 \\ \underline{391000.000} \pm 1900.000 \end{array}$	93.252 ± 0.886 78.178 ± 6.179 80.845 ± 4.087	$\begin{array}{c} -54.955 \pm 33.482 \\ 540.603 \pm 20.205 \\ 567.042 \pm 11.653 \end{array}$	$\begin{array}{c} 226.491 \pm 21.120 \\ 277.888 \pm 7.799 \\ \underline{285.110 \pm 15.130} \end{array}$
CbAS MINs DDOM Ours	0.958 ± 0.018 0.938 ± 0.047 0.971 ± 0.005 0.990 ± 0.003	$\begin{array}{c} 0.761 \pm 0.067 \\ 0.770 \pm 0.177 \\ \underline{0.885 \pm 0.367} \\ \textbf{1.344 \pm 0.340} \end{array}$	$\begin{array}{c} 389000.000\pm500.000 \\ 390950.000\pm200.000 \\ 387950.000\pm1050.000 \\ 392149.225\pm3821.853959 \end{array}$	83.178 ± 15.372 89.469 ± 3.227 103.600 ± 8.139 104.848 ± 3.113	$\begin{array}{c} 468.711 \pm 14.593 \\ 533.636 \pm 17.938 \\ 548.227 \pm 11.725 \\ \underline{572.490 \pm 7.277} \end{array}$	$\begin{array}{c} 213.917 \pm 19.863 \\ 272.675 \pm 11.069 \\ 250.529 \pm 10.992 \\ \textbf{293.327} \pm \textbf{7.452} \end{array}$

50-th percentile results We present the normalized results with Q=256 at 50-th percentile to further demonstrate the effectiveness of our approach in Tab. A7.

Table A7: Normalized results on design-bench. 50-th percentile results with Q=256. Baseline numbers from [19]. DDOM [11] does not report 50-th percentile results; we are unable to find public model weights corresponding with the results in Tab. 2 for DDOM and therefore omit DDOM in this table.

BASELINE	TFBIND8	TFBIND10	CHEMBL	SUPERCON.	ANT	D'KITTY	MEAN SCORE [↑]	$\mathbf{MNR}^{\downarrow}$
GP-qEI CMA-ES REINFORCE	$\begin{array}{c} 0.443 \pm 0.004 \\ 0.543 \pm 0.007 \\ 0.450 \pm 0.003 \end{array}$	$\begin{array}{c} 0.494 \pm 0.002 \\ 0.483 \pm 0.011 \\ 0.472 \pm 0.000 \end{array}$	$\begin{array}{c} 0.299 \pm 0.002 \\ 0.376 \pm 0.004 \\ 0.470 \pm 0.017 \end{array}$	$\begin{array}{c} 0.272 \pm 0.006 \\ -0.051 \pm 0.004 \\ 0.146 \pm 0.009 \end{array}$	$\begin{array}{c} 0.754 \pm 0.004 \\ 0.685 \pm 0.018 \\ 0.307 \pm 0.002 \end{array}$	$\begin{array}{c} 0.633 \pm 0.000 \\ 0.633 \pm 0.000 \\ 0.633 \pm 0.000 \end{array}$	$\begin{array}{c} 0.491 \pm 0.016 \\ 0.466 \pm 0.020 \\ 0.083 \pm 0.004 \end{array}$	4.8 5.2 5.7
Gradient Ascent COMs BONET	$\begin{array}{c} 0.572 \pm 0.024 \\ 0.492 \pm 0.009 \\ 0.505 \pm 0.055 \end{array}$	0.470 ± 0.004 0.472 ± 0.012 0.496 ± 0.037	$\begin{array}{c} 0.463 \pm 0.022 \\ 0.365 \pm 0.026 \\ 0.369 \pm 0.015 \end{array}$	$\begin{array}{c} 0.141 \pm 0.010 \\ 0.525 \pm 0.018 \\ 0.819 \pm 0.032 \end{array}$	$\begin{array}{c} 0.637 \!\pm\! 0.148 \\ 0.885 \!\pm\! 0.002 \\ \textbf{0.907} \!\pm\! \textbf{0.020} \end{array}$	$\begin{array}{c} 0.633 \pm 0.000 \\ 0.633 \pm 0.000 \\ 0.630 \pm 0.000 \end{array}$	$\begin{array}{c} 0.478 \pm 0.029 \\ 0.522 \pm 0.034 \\ 0.614 \pm 0.035 \end{array}$	5.1 4.6 3.4
CbAS MINs Ours	0.422 ± 0.007 0.425 ± 0.011 0.896 ± 0.033	0.458 ± 0.001 0.471 ± 0.004 0.507 ± 0.012	0.111 ± 0.009 0.330 ± 0.011 0.373 ± 0.002	0.384 ± 0.010 0.651 ± 0.010 0.715 ± 0.004	0.752 ± 0.003 0.890 ± 0.003 0.907 ± 0.008	0.633 ± 0.000 0.633 ± 0.000 0.630 ± 0.000	0.436 ± 0.008 0.547 ± 0.005 0.672 ± 0.009	6.5 4.8 1.2

25-th, 50-th and 75-th percentile results We present the normalized results with Q=128 at 50-th percentile to further demonstrate the effectiveness of our approach in Tab. A9. Additionally, we provide results at 25-th and 75-th percentiles for reference in Tab. A8.

Table A8: Normalized design-bench 25-th and 75-th results with Q = 128.

Percentile	TFBIND8	TFBIND10	SUPERCON.	ANT	D'KITTY
25-th	0.635 ± 0.020	0.453 ± 0.007	0.351 ± 0.019	0.527 ± 0.033	0.878 ± 0.002
75-th	0.873 ± 0.006	0.945 ± 0.012	0.409 ± 0.013	0.832 ± 0.012	0.910 ± 0.002

Table A9: Normalized design-bench 50-th percentile results with Q=128. Baseline numbers from [12, 18, 20, 22]. **ChEMBL** dataset is excluded following baseline set-ups. * indicates that the baseline has slightly different set-ups; the numbers are for rough reference (see Appx. E.2.3 for more details).

BASELINE	TFBIND8	TFBIND10	SUPERCON.	ANT	D'KITTY	MEAN SCORE [↑]	MNR↓
\mathcal{D} (best)	0.439	0.467	0.399	0.565	0.884	-	-
GP-qEI	0.439 ± 0.000	0.467 ± 0.000	0.300 ± 0.015	0.567 ± 0.000	0.883 ± 0.000	0.531	11.2
CMA-ES	0.537 ± 0.014	0.484 ± 0.014	0.379 ± 0.003	-0.045 ± 0.004	0.684 ± 0.016	0.408	10.2
REINFORCE	0.462 ± 0.021	0.475 ± 0.008	0.463 ± 0.016	0.138 ± 0.032	0.356 ± 0.131	0.379	10.8
*BOOTGEN	0.833 ± 0.007	-	-	-	-	-	-
*ExPT	0.473 ± 0.014	0.477 ± 0.014	-	0.705 ± 0.018	0.902 ± 0.006	-	-
Grad. Ascent	0.532 ± 0.017	0.529 ± 0.027	0.339 ± 0.015	0.564 ± 0.014	0.877 ± 0.005	0.568	7.4
COMS	0.439 ± 0.000	0.466 ± 0.002	0.316 ± 0.022	0.568 ± 0.002	0.883 ± 0.002	0.534	10.6
BONET	0.505 ± 0.004	0.465 ± 0.002	0.470 ± 0.004	0.620 ± 0.003	0.897 ± 0.000	0.591	5.4
ROMA	0.555 ± 0.020	0.512 ± 0.020	0.372 ± 0.019	0.479 ± 0.041	0.853 ± 0.007	0.554	7.6
NEMO	0.548 ± 0.017	0.516 ± 0.020	0.322 ± 0.008	0.593 ± 0.000	0.885 ± 0.000	0.539	10
BDI	0.439 ± 0.000	0.476 ± 0.000	0.412 ± 0.000	0.474 ± 0.000	0.855 ± 0.000	0.546	9.4
IOM	0.439 ± 0.000	0.477 ± 0.010	0.352 ± 0.021	0.509 ± 0.033	0.876 ± 0.006	0.531	9.8
ICT	0.551 ± 0.013	0.541 ± 0.004	0.399 ± 0.012	0.592 ± 0.025	0.874 ± 0.005	0.591	5.2
Tri-mtring	0.609 ± 0.021	0.527 ± 0.008	0.355 ± 0.003	0.606 ± 0.007	0.886 ± 0.001	0.597	4.2
CbAS	0.428 ± 0.010	0.463 ± 0.007	0.111 ± 0.017	0.384 ± 0.016	0.753 ± 0.008	0.428	15
Auto.CbAS	0.419 ± 0.007	0.461 ± 0.007	0.131 ± 0.010	0.364 ± 0.014	0.736 ± 0.025	0.422	15.8
MINs	0.421 ± 0.015	0.468 ± 0.006	0.336 ± 0.016	0.618 ± 0.040	0.887 ± 0.004	0.546	8.8
DDOM	0.553 ± 0.002	0.488 ± 0.001	0.295 ± 0.001	0.590 ± 0.003	0.870 ± 0.001	0.559	8.6
Ours	0.873 ± 0.006	0.499 ± 0.002	0.370 ± 0.004	0.704 ± 0.013	0.897 ± 0.003	0.669	3

Extended discussion for ablation study

MLE vs. NTRE We term the LEBM learned by MLE as the MLE-LEBM in Tab. 4. We present scores for MLE-LEBM and our model obtained with both LD and SVGD for analysis. We observe that the vanilla MLE learning paradigm for LEBM performs poorly in the offline BBO set-up. We conjecture that this is because the joint latent space of \mathbf{x} and y can have a complex landscape, in which short-run MCMC can be severely biased, resulting in an inaccurately estimated density model. This can be seen in the significant performance gap between MLE-LEBM w/ LD and MLE-LEBM w/ SVGD, as SVGD is more robust to the highly multimodal landscape. In contrast, we can see that our model learned by Eq. (9) produces decent results even with LD sampling, indicating a better-learned and well-shaped latent space compared with MLE-LEBM.

Gaussian vs. LEBM One may argue that a simpler prior model such as Gaussian prior might be enough to tackle this problem. To demonstrate the necessity of an informative prior, we train a Gaussian-prior VAE with Eq. (1) to ablate the learnable prior model p_{α} . We observe that models trained with non-informative Gaussian prior obtain similar results when sampled with LD or SVGD. This indicates that the joint latent space is regularly shaped (approximate unimodal due to the Gaussian prior), but it can be over-regularized by the Gaussian prior as it does not encode enough information for the correlation between \mathbf{x} and y, unlike our method. LEO not only achieves descent results with LD sampler, but also demonstrate significant improvements when using SVGD sampler. It implies a good balance between the regularity of the induced latent space landscape and the amount of information encoded in it.

LD vs. SVGD We compare the results of each model using both LD and SVGD samplers. The vanilla LD sampling refers to short-run LD initialized from $\mathcal{N}(0,\mathbf{I})$. We can see in Tab. 4 that sampling with SVGD shows consistently better scores of the listed models, compared with vanilla LD sampling. The improvement is especially significant for the LEBM learned through MLE. The LEBM trained by NTRE objective achieves decent result with LD sampler; the performance is further boosted with SVGD sampler. The Gaussian prior model shows slightly better result using SVGD sampler compared with LD sampler. These results together indicate that SVGD sampler is suitable for sampling-based optimization in the latent space, and especially more effective when the density is multimodal: it benefits from its particle-based update rule and shows a stronger ability traversing among different modes.

Hyperparameters As mentioned in Sec. 4.3, we provide ablative results on noise intensity M, number of intermediate stages K+1 and query budget Q in Tabs. 4 to 6. Of note, the K+1=1, M = 100 row in Tab. 4 means learning a LEBM w/ Eq. (9) alone, w/o ratio decomposition. We can see that the variant delivers significantly better results than MLE-LEBM w/ SVGD sampler. This indicates the effectiveness of the noise-intensified objective. K+1=6, M=1 row means learning with the original TRE objective, w/o intensifying the noise distributions. We can see that simply combining the original TRE objective with variational learning of LEBM only achieves inferior performance compared with learning LEBM with the NTRE objective. We further provide detailed ablation of M in Tab. 5. We can see that greater M, e.g., M = 100 or M = 1000 is significantly better than smaller M, e.g., M=1 or M=10. However, larger M also incurs larger memory consumption based on our implementation in Appx. D. We therefore choose M=100 for all experiments. These results further confirm our assumption about the noise intensity. We can see from Tab. 5 that larger number of intermediate stages K+1 typically brings better performance. These results demonstrate the need for ratio decomposition. In addition, since we are using the same network architecture for ablating different Ks, the network capacity is fixed. Larger number of intermediate stages may require a larger network to perform well (circumventing competition between stages), as we are learning the ensemble of ratio estimators using the shared network. SVGD in the data space typically requires a relatively large population of initial samples to perform well. In our set-up, we set the query budget Q to the population size and run SVGD in the latent space. We can see from Tab. 6 that LEO is robust to Q by pulling SVGD sampling back to the latent space.

Random baselines One valid concern is that our framework LEO solves the offline BBO problem by simply memorizing the best points in the offline dataset and proposing new points close to those best points during evaluation utilizing the randomness in the sampling process. To see whether this is the case, we follow Mashkaria et al. [19] to perform a simple experiment on the **D'Kitty** task. We include random baselines by similarly choosing a small hypercube domain around the optimal point in the offline dataset. These baselines then uniformly sample 256 random points in the cube as the proposed candidates; this can be seen as a offline dataset oracle w/ noise model. In Tab. A10, we show the results for different widths of this hypercube ranging from 0 to 0.1. 0 width means returning the best point in the offline dataset. We can see that the best result (226.10) from these noisy oracle models is significantly lower than the result from our model (304.36). We can also see from the trend in max, mean and std. values that simply extending the width of cube for random search is hopeless for solving the offline BBO task. This is very likely due to the high-dimensionality and highly-multimodal nature of the black-box function input space. The comparison between these random baselines and our method suggests that LEO does find an informative latent space for effectively extrapolating beyond the offline dataset best designs. The prior model in our formulation provides meaningful gradient for exploring the underlying high-function-value manifold.

Table A10: Random baseline results on the D'Kitty dataset. Results from 5 runs.

CUBE WIDTH	0.00	0.005	0.01	0.05	0.1	OURS
Max [↑]	199.23	212.66	222.44	226.10	209.00	304.36
Mean [↑] Std.↓	199.23 0.00	190.68 9.28	182.13 12.21	-169.62 331.00	-368.71 261.37	$206.76 \\ 63.26$

F Further Discussion

F.1 Limitations and Future Work

After training, we employ gradient-based samplers such as SVGD and LD to perform sampling-based optimization. It would be great to have the convergence rate (or sampling quality) analysis of SVGD and LD samplers, which is also an interesting and active research area with abundant on-going works (*e.g.*, [103]). This is however outside the scope of this work. We would like to further investigate this direction in the future if needed.

Another direction for potential improvement is the time efficiency. Currently our framework requires gradient-based sampling for optimization, with a resulting sampling speed similar to diffusion-based baselines, *e.g.*, DDOM [11]. While sampling speed is typically not a major bottleneck for offline BBO, it can be potentially limiting for some real-time applications. We expect techniques such as learning amortized samplers [31] to be transferred to our framework in future works. Finally, we focus extensively on offline BBO in this work, it might be interesting to consider the online learning scheme of our model for active data acquisition for solving online BBO problems.

F.2 Broader Impacts

Our framework focuses on solving the BBO problem. Though we consider our work not tied to particular applications or deployments, it is possible that more powerful models augmented with this framework may be used maliciously. One potential negative impact could be the misuse of this technology in designing objects or entities for harmful purposes such as harmful biological agents. Work on appropriate safeguards and regulations could be important to address such harms.